LLTR-89-1

IMAGE-BASED TERRAIN MODELING WITH THEMATIC MAPPER

APPLIED TO RESOLVING THE LIMIT OF HOLOCENE LAKE EXPANSION

IN THE GREAT SALT LAKE DESERT, UTAH

By

John A. Merola

NASA Contract NAS5-28753, Final Report, Part I

Limneotectonics Laboratory Technical Report 89-1

July 25, 1989

Department of Geography

University of Utah

Salt Lake City, Utah 84112

IMAGE-BASED TERRAIN MODELING WITH THEMATIC MAPPER

APPLIED TO RESOLVING THE LIMIT OF HOLOCENE LAKE EXPANSION

IN THE GREAT SALT LAKE DESERT, UTAH

By

John A. Merola

Department of Geography

University of Utah

Salt Lake City, Utah   84112

ABSTRACT

The Landsat Thematic Mapper (TM) scanner records reflected solar energy from the earth's surface in six wavelength regions, or bands, and one band that records emitted energy in the thermal region, giving a total of seven bands. The goal of this research has been to extract useful information about terrain morphometry from remote sensing measurements and to use this information in an image-based terrain model for selected costal geomorphic features in the Great Salt Lake Desert (GSLD).

Technical developments include the incorporation of Aerial Profiling of Terrain System (APTS) data in satellite image analysis, and the production and use of three-dimensional surface plots of TM reflectance data. Also included in the technical developments is the analysis of the ground control point spatial distribution and its affects on geometric correction, and the terrain mapping procedure; using satellite data in a way that eliminates the need to degrade the data by resampling.

The most common approach for terrain mapping with

multispectral scanner data includes the techniques of pattern recognition and image classification, as opposed to direct measurement of radiance for identification of terrain features. The research approach in this investigation has been based on an understanding of the characteristics of reflected light resulting from the variations in moisture and geometry related to terrain as described by the physical laws of radiative transfer. The image-based terrain model provides quantitative information about the terrain morphometry based on the physical relationship between TM data, the physical character of the GSLD, and the APTS measurements.

TABLE OF CONTENTS

PRECEDING PAGE BLANK NOT FILMED

LIST OF TABLES

LIST OF FIGURES

x

CHAPTER 1

INTRODUCTION

1.1 Objective

The objective of this research is to develop a quantitative model of selected coastal geomorphic features in the Great Salt Lake Desert using remote sensing measurements. The modeling of selected coastal geomorphic features has provided data that was used to map the potential limits of prehistoric expansion of the Great Salt Lake into the Great Salt Lake Desert (GSLD).

The Thematic Mapper (TM) multispectral scanner is the primary measurement device involved in this research. This remote sensing device is on board the Landsat 4 and Landsat 5 satellites. The TM scanner records reflected solar energy from the earth's surface in six wavelength regions, or bands, of the electromagnetic spectrum. The TM scanner also has one band that records emitted energy in the thermal region, giving a total of seven bands. Nominal ground resolution for the reflected bands is 30 meters-square, for each pixel (picture element) and 120 meters-square for the thermal band. A second remote sensing device involved in this investigation is the Aerial Profiling of Terrain

System (APTS). APTS was developed by the Charles Stark Draper Laboratory, Inc., Cambridge, Massachusetts, for the U.S. Geological Survey. The APTS is an airborne inertial surveying system supplemented with laser instruments which provide measurements for transferring position and elevation coordinates to the ground. The laser profiler and laser tracker can perform terrain mapping tasks to accuracies of $\pm$ 15 cm (1/2 foot) vertically and $\pm$ 61 cm (2 feet) horizontally. The APTS is installed in a De Havilland Twin Otter aircraft.

1.2 Context of the Investigation

The approach being employed by many researchers in remote sensing is based 'on an understanding of the physical radiative interactions with materials on the Earth's surface. As stated by Smith (1983) in the Manual of Remote Sensing (2nd Ed. 1983, p. 64) "the fundamental measurable remote-sensing quantity for a scene element is its spectral radiance." Scene elements in this context are synonymous with elements of the terrain that can be resolved by the multispectral scanner.

Image-based models are founded on recorded radiance of scene elements. The techniques of pattern recognition and image classification are frequently used to map landcover/landuse, as opposed to direct measurement of

radiance for identification of scene elements. Mapping of landcover/landuse is attempted through correlation between the variables comprising landcover/landuse and various spectral classes derived from statistical recognition of pattern. Because of variability induced into the radiance measurements from such factors as differing terrain, moisture characteristics and illumination geometries, regression techniques are used to establish the relationship between elements of landuse/landcover and spectral classes. Also, the mapping of landuse/landcover is accomplished by using predictive relationships between techniques that transform the radiance values and empirical investigation. The transformation of radiance values include the techniques of band ratios and vegetation indices.

During the last decade many models have been developed to derive information about terrain from digital remote sensing data. The multispectral scanner on board Landsat satellites 1 through 3, referred to as the MSS, were used in many of these investigations. The MSS records reflected light in four spectral bands as opposed to the seven bands of the TM scanner. Due to eight-bit quantizing the TM scanner has an improved dynamic range, 0 - 255, as opposed to the six-bit quantizing, 0 - 63, dynamic range of MSS. TM also has an increased spatial resolution of 30 meters, as compared to the 79 meters of the MSS.

Eliason et al. (1981) and Campbell et al. (1984) developed techniques of modeling topography from MSS data. Eliason et al. (1981) used variation in reflected light to extract topographic information from MSS digital imagery. This approach is closed in that it uses only information contained within the image itself. The authors suggest that this technique can be used in mitigating the effects of topography on reflected light for improved image interpretation and classification. Eliason et al. (1981) also used this technique to create a subjective stereoscopic display of the image. Campbell et al. (1984) modified the technique of Eliason et al. (1981) to develop a procedure that approximates the relief of the topography within an MSS image. This technique was applied to the identification of ridges and valleys to construct a representation of the drainage network. The authors advocate the use of interpreted topography from MSS data in quantitative hydrologic models.

Shih and Schowengerdt (1983) used the addition of image texture (tone and spatial variability) to improve the classification of arid geomorphic surfaces from MSS imagery. This texture feature, derived from the imagery itself, is not directly related to ground surface texture; however, when added to the analysis of the imagery it improved the classification of arid geomorphic surfaces significantly. The results of this technique provide data

that is two dimensional, in map form, and provides little information about the morphometry of the terrain.

Reflectance modeling in sparse vegetation canopies and soil reflectance models provide a physical basis for research involving multispectral scanners as measurement devices. Colwell (1981) produced a three-dimensional model to determine plant cover from MSS reflectance. In Colwell's three-dimensional model of desert vegetation, plant cover is modeled using field measurements of reflected light from bare soil, erect stems and their shadows. Ustin et al. (1985) describe the spectral characteristics of semi-arid shrubs and soils, their results provide field information and an understanding of the light reflectance characteristics of shrubs and soils within the Great Basin. Tucker et al. (1985) studied the reflectance of soil and vegetation in arid areas of Northern Africa. Other research pertaining to reflectance in sparse vegetation canopies includes that by Huete et al. (1985), Cooper and Smith (1985), Kimes et al. (1985), Elvidge and Lyon (1985), and Becker et al. (1984).

Research in sun-view angle and directional reflectance factors increase the understanding how light reflects from scene elements, given known terrain characteristics. Norman et al. (1985) provides much insight into the apparent brightness of natural surfaces as they relate to the direction of the incident radiation, viewing direction, and

the surface shape. Li and Strahler (1985) found that shape, form, and shadowing of objects within a pixel have a major impact on reflected light received by the detectors of multispectral scanners. The research of Kimes (1983) dealt with directional reflectance factors over a variety of vegetation canopies and bare soil. Ranson et al. (1985), Shibayama and Wiegand (1985), Kimes et al. (1984), and Wardley (1984) also investigated illumination-viewing geometry. Eaton and Dirmhirm (1979) studied the direction reflectance of the Bonniville Salt Flats under various illumination geometries. The area of mathematical modeling of plant canopies has received much attention and two complete reviews of these models are given in Bunnik (1984) and Smith (1983).

The characteristics of reflected light resulting from the variations in moisture and geometry related to terrain can be understood through the physical laws of radiative transfer. This dissertation attempts to measure morphometry of geomorphic features through the study and understanding of the reflectance characteristics from terrain.

1.3 Field Characteristics

The Great Salt Lake Desert (GSLD) was selected as the study area because of the opportunity to study costal geomorphic features. This area is within the Great Basin

physiographic province. The largest individual basin within the Great Basin includes the GSLD and the Great Salt Lake. The GSLD is a large basin-floor desert, located west of the Great Salt Lake (Curry, 1980). The study area location is shown in Figure 1. Figure 1 indicates the general area for which the TM terrain model was developed.

The floor of the GSLD is geomorphically similar to a large gently shelving costal plain; the topography is very flat below an elevation of about 1286 meters (4218 feet) above sea level. The floor of the GSLD is predominately saline mud flat. Around the perimeter, and in some internal areas, arid and costal eolian geomorphic processes dominate. The expression of the above eolian processes include sand dunes, loessal regolith covering paleo-costal and fluvial features, and erosional features such as earlier eolian depositional features that have since been deflated.

The most recent expansions of the Great Salt Lake, during late Holocene time (the most recent 2,000 years of earth history), were too shallow to permit the propagation of large, energetic waves into the shore zone. The result of the low-energy erosion is a pattern of partially removed older surficial materials. This pattern is characterized by a moderately distinct trimline-like limit around the margins of sand dunes where the sand dune meets the basin-floor.
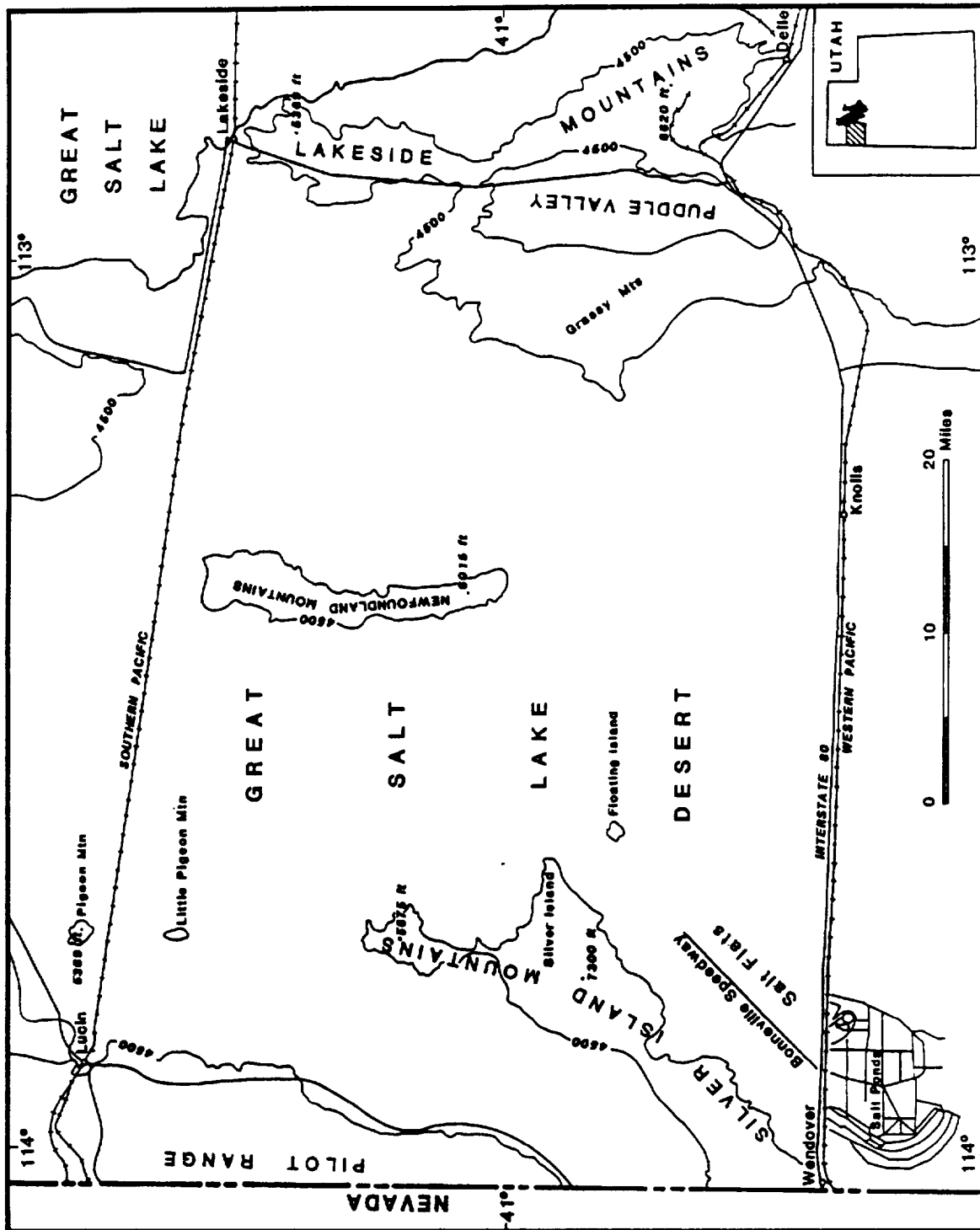
Figure 1. Study area location map. The TM terrain model was developed for geomorphic features within the GSLD below the elevation of 4500 feet.

Flowers and Evans (1966) gives this description of the GSLD:

" This vast playa was the last extensive basin vacated by Great Salt Lake in its decline. Most of the surface is white with a crust of salt covering the yellowish or gray clays or forming a fluffy mixture of loose clay and crystals. At wide intervals the flat surface is interrupted by sinuous wave-wrought terraces upwards to two meters high. During the summer, heat waves shimmer over the desert and mirages are a constant feature. The area is subject to wind erosion and large amounts of salt are removed during storms. The wind has also built non-calcareous sand dunes at some points around the margins and on some of the larger terraces in mid-desert. The average annual rainfall over the area is about 11 cm. By summer the surface becomes very dry, although in most places the water-table is 1-2 m below the surface. Some places are entirely barren, without even an occasional plant to interrupt the monotony of the white surface. However, the area as a whole is far from being entirely barren, as Allenrolfea [Iodinebush] has become established on higher ground around the margins and on isolated hummocks of wind blown soil formed around tumbleweeds and other objects far out on the flats. The usual hummocks also form round the branches of the shrubs and in time the salt leaches from them, permitting an occasional plant of Suaeda torreyana [Bush Seepweed], Sarcobatus vermiculatus [Greasewood] or Atriplex nuttallii [Saltbush] to grow on the hummock also."

1.4 Statement of Hypothesis

Hypothesis: Through the analysis of the multi-dimensional data structure of TM, extraction of useful information about terrain morphometery is possible.

Geomorphologic classification of terrain from multispectral imagery has been restricted to a two

dimensional approach until recently. Shih and Schowengerdt (1983) classified surface geomorphology as to its spatial and spectral patterns, the result of which is a map showing only the spatial extent of features. The above approach does not fully incorporate the multi-dimensional data content in the multispectral image. By exploring the information content in the uncomplicated landscape of the GSLD, this dissertation addresses the complicated question of multi-dimensional data structure in multispectral imagery.

Determining the multi-dimensional data structure of TM imagery requires an investigation of both the spectral and spatial attributes inherent in these data. To simply say that the spatial resolution is that of the pixel resolution (30 meters-square) is to ignore the radiometric sensitivity of TM data which may contain information about features smaller than 30 meters-square.

The TM records the spectral response of each band to reflected light from the earth's surface as a digital value (DV). The DV for a given pixel in a given band is a integrated signal of reflected light resulting from all components of the landscape, including the morphometry of the terrain. Within a pixel, the factors influencing the reflectance are: 1) the materials involved - rock, soil, vegetation; 2) the physical state of the components - from dry to wet, light to dark color, non-vigorous to vigorous

vegetation growth; 3) the dimensions of the components-size, shape, orientation to the sun, and distribution. The dimensions of a pixel include the X,Y spatial coordinates as well as the DV for each of the TM bands. The focus of this dissertation is determining the morphometry of the terrain as represented by the several DVs' of a pixel given its spatial context.

1.5 Experimental Approach

Careful analysis of the information content of TM data begins with an understanding of the structure of the data. The quality and quantity of information contained in the structure is a result of the attributes of the sensor and the characteristics of the terrain which the data represent. The attributes of the TM sensor give it the ability to resolve and record spectral and spatial information about terrain and a study of the data structure allows one to find the expression of physical characteristics of terrain in the data.

Understanding the multi-dimensional data structure of TM data requires some insight into the relationship of the terrain to the data structure. To this end, the experimental approach begins with the selection of several sample areas for image analysis and field survey. Reconnaissance field data were collected from several

sample field locations; these data include photographs, observations of the terrain, profile measurements, and soil samples. The Silver Island area was selected for more intense study because of the reliability of the APTS profile that runs through the selected sample area, and the existence of a trimline where the sand dune perimeter of Silver Island meets the GSLD basin-floor. The field survey included a detailed topographic profile made along the APTS profile using a Lietz/Sokkisha B1C automatic level. Vegetation and soil data were also collected along the profile and from two transects, on each side of the profile.

Understanding the structure of TM data involved viewing the data in several forms of graphic displays. In discussing their approach to understanding the data structure of MSS, Kauth and Thomas (1976) wrote:

> The first step is to find a variety of ways to display the data. Given the displays, one will notice the structure of the data, will name the data structure, will create some visual model of the data structure. Such a model may suggest a physical interpretation or a quantitative test. One then subjects the description to quantitative test, resulting in gradual elaboration and refinement of the description, or, in some cases, in its destruction.

Displays used in this research included viewing the reflectance of each band as a surface. This display developed from the use of two dimensional line plots, of each band, over selected terrain of interest. The line plots were produced by selecting areas where the row or

column pattern of the image corresponded with the orientation of the terrain, (i.e., a line plot would have the row or column (depending on the orientation of the terrain) number as the X axis and the DV for a TM band on the Y axis of the plot). The three dimensional perspective plot was used to provide a better view the reflectance surface than the line plot. Viewing three dimensional reflectance surface allowed for an analysis of complex and subtle interactions between terrain and reflectance. Three dimensional perspective plots have the image column number for the X axis, the row number for the Y axis, and the DV for individual bands as the Z axis. Other displays used included: gray tone image of individual bands, a three-color composite, and scatter plots of the TM band combinations. The analysis of these displays of TM data lead to a greater understanding of multi-dimensional data structure and indicated the potential for quantitative analysis of the data.

Quantitative analysis of the TM data included the use of image filters and image transformations to focus on that portion of the data structure which pertained to topographic information. These procedures where used to enhance the information of interest and to reduce the amount of information and 'noise' that is not useful or obscures the information of interest. There is a balance that needs to be maintained during these procedures between

information enhancement and information loss.

Digital elevation profiles obtained from the APTS provide the field survey information used to develop a quantitative model of topography from digital TM data. Unprocessed TM data, as well as the results of each image processing technique, were compared to the APTS data in attempts to correlate with the topography. Calibration of the model, topographic reference, and verification of the detection of micro-relief are obtained from the APTS profiles.

Finally, the model will result in the ability to observe, relate, quantitatively describe, and classify geomorphic features using digital TM data and digital APTS elevation profiles.

CHAPTER 2

THEMATIC MAPPER DATA PROCESSING

2.1 Introduction

The Landsat Thematic Mapper (TM) is an advanced multispectral scanning remote sensing system. The TM measures the intensity of radiation from the Earth's surface in selected portions of the electromagnetic spectrum, as mentioned earlier. This scanner is carried aboard the Landsat satellites 4 and 5. These satellites travel in a near-polar orbit that is sun synchronous, at a altitude of 705 km. Landsat satellites 4 and 5 cross the equator at approximately 9:45 a.m. local solar time during the descending (north-to-south) portion of each orbit in the Northern Hemisphere. This orbital configuration enables just over 14.5 orbits a day, with the result that the satellite will overpass the same ground location every 16 days. The ground resolution for the six reflective spectral bands is 30m by 30m (bands 1, 2, 3, 4, 5, and 7) and 120m by 120m for the thermal band (band 6). Table 1 lists the spectral resolution of the seven TM bands along with the rational for selecting each band.

One of the most important sensor capabilities of the

TABLE 1

THEMATIC MAPPER SPECTRAL BANDS
(MODIFIED FROM SALOMONSON ET AL., 1980)

BAND	BAND WIDTH*	SELECTION RATIONAL
1	0.45 - 0.52	Sensitive to chlorophyll and cartonoid concentrations for differentiation of soil-- vegetation and deciduous-- conifer forest, as well as, coastal water mapping.
2	0.52 - 0.60	Sensitive to green reflectance by healthy vegetation.
3	0.63 - 0.69	Sensitive to chlorophyll absorption for plant species differentiation.
4	0.76 - 0.90	Sensitive to near infrared reflectance of healthy vegetation for biomass surveys.
5	1.55 - 1.75	Sensitive to vegetation moisture and snow/cloud cover reflectance differences.
6	10.4 - 12.5	Thermal mapping.
7	2.08 - 2.35	Sensitive to vegetation moisture and to hydroxyl ions in minerals for geological mapping.

* Values are in micrometers

TM is the in-flight radiometric calibration data collected along with multi-spectral data. In-flight radiometric calibration data are combined with pre-launch calibration, at ground facilities, and TM digital values are converted into absolute radiometric units (e.g., milliwatts per square centimeter per steradian per micrometer). Radiometric correction procedures enable the consistent and quantitative measurement of spatial and temporal spectral variations in TM imagery. The TM scanner on Landsat 4 has two malfunctioning detectors; the third detector of band 5 has no radiometric response and the fourth detector of band 2 has poor spatial resolution. Digital values from each malfunctioning detector are replaced from an adjacent detector, in the same band, during radiometric processing on the ground. There are 16 detectors in the six reflective bands (bands 1 to 5 and band 7) and four detectors in thermal band (band 6). All of the detectors of the TM scanner on Landsat 5 are working properly.

The above information was provided by NASA's Landsat Image Data Quality Analysis (LIDQA) program, which produced publications that include the Proceedings of the Landsat 4 Science Characterization Early Results Symposium (1983), the NASA Technical Memo on TM research (1984), and two special issues of the Institute of Electrical and Electronic Engineers (IEEE) Transactions on Geoscience and Remote Sensing, April 1980 and May 1984, as well as the

special LIDQA issue of Photogrammetric Engineering and Remote Sensing, September 1985. The overall conclusion of the LIDQA program is that the quality of the data received from the TM sensors on Landsat 4 and 5 is very good. The LIDQA program evaluated the radiometric and geometric quality of the TM data. TM data received from the Earth Resources Observation System (EROS) Data Center, in the computer compatible tape (CCT-PT) format, for this study have a high radiometric and geometric quality, with errors close to those targeted in sensor design specifications (Walker et al., 1984).

The overall radiometric quality of the data is good; however, there is noise in the data unrelated to scene phenomena. It is important to understand the sensor radiometric characteristics so that sensor related noise is not confused with actual scene phenomena (Malila and Metzler, 1984). It is also desirable to correct, to the extent possible, the noise in order to extract the maximum information.

Two dates of imagery were used in this research: July 2, 1984 and June 19, 1985. On July 2, 1984 the solar elevation was 60 degrees and the azimuth was 116 degrees, while on June 19, 1985 the solar elevation was 61 degrees and the azimuth was 117 degrees. These solar elevations and azimuths are considered to be constant throughout the entire TM image. The maximum angle of any given target in

the GSLD from the nadir (center) of the images is five degrees. Given this fact all targets are assumed to be at or nearly at nadir, i.e., the satellites are essentially directly overhead of all targets in the GSLD.

With the solar elevation as high as 60 degrees, view angles ranging between 85 and 90 degrees, and very little abrupt topography (below an elevation of 1285 meters (4218 feet)), the influence of shadowing and view angle on the TM data is considered to be negligible.

2.2 Geometric Registration

Geometric registration of the TM image is necessary for the following reasons: 1) band-to-band registration, 2) geodetic registration, 3) temporal registration. It is important to have band-to-band registration so a pixel from one band in the image is correctly overlaid on the same pixel from another band. Geodetic registration is important for the determination of the cartographic location of a TM pixel accurately from the pixel's row/column image coordinates. Temporal registration is used to accurately overlay two TM image acquired over the same geographic area on different dates.

Band-to-band registration is accomplished prior to receiving the data from the EROS data center. To properly register the seven TM bands, in which some bands are

unevenly spaced, each pixel in each band is resampled from the original 30m by 30m area to an evenly-spaced grid where each pixel represents a 28.5m by 28.5m area on the earth's surface. The resampling procedure assigns a digital value to the resulting pixel on the basis of interpolation of the original pixel value and the neighboring pixels.

Geodetic registration was accomplished at the Center for Remote Sensing and Cartography, University of Utah Research Institute, Salt Lake City, Utah, where all subsequent data processing took place. Processing and analysis of the TM imagery was accomplished using ELAS (Earth Resources Laboratory Applications Software) operating on a Prime 2655 computer. ELAS is a geobased information subsystem developed by NASA's National Space Technology Laboratories, Earth Resources Laboratory. ELAS is designed for analyzing and processing digital data in a grid cell format such as digital imagery collected by multispectral scanners or digitized maps (Graham et al. 1980).

Geodetic registration requires identification of as many ground control points (GCP) as can be gathered (e.g., for the July 2, 1984 image, 312 GCPs were collected). A GCP is a recognizable feature common to both the TM image and the reference map to which the image is to be registered. In this study goedetic registation was accomplished using the Universal Transverse Mercator (UTM) coordinate system.

The GCPs are used to derive mapping coefficients that are used to calculate the UTM coordinate for any TM pixel. Mapping coefficients approximate TM pixel line(row) and element(column) as linear functions of UTM easting(X) and northing(Y), as in the following equations:

(2) $L = A_1 + A_2X + A_3Y$

(3) $E = B_1 + B_2X + B_3Y$

where

L is the TM pixel line(row)
E is the TM pixel element(column)
X is the UTM easting
Y is the UTM northing
The A's and B's are the mapping coefficients.

(Graham et al., 1980)

2.3 Light Reflectance and Soil Moisture

In the discussion on the application of remote sensing data to soil-moisture determination, Salomonson et al. (1983) states:

"...much research has been accomplished which shows clearly that observations are sensitive to variations in soil moisture. In addition, the fundamental physical principles influencing remotely sensed observations are well understood." p. 1507

Physical interactions occurring between soil moisture at or near the surface and incoming solar radiation are most likely responsible for the ability of TM to discriminate micro-relief in the GSLD. Micro-relief of landforms resulting from past and present geomorphic processes in the

GSLD appear to have drier surfaces than the extensive mudflats of the basin-floor. This may be due to the fact that the surfaces of the landforms have a greater distance to the water table than the surface of the basin-floor. Most likely, the interaction between micro-relief and soil moisture leads to a phenomena that allows for the detection and measurement of micro-relief.

TM band 7 was specifically designed to be sensitive to moisture content in vegetation and soil, and to hydroxyl ions in minerals for geological mapping (Salomonson et al., 1980). Figure 2 shows the clear water absorbance characteristics of the six TM reflective bands.

In chapter 3.3 of Crist et al. (1984), Measuring Soil Moisture in the TM Band Wavelengths, the response of reflectance in the TM bands 1 to 5 and 7 to variations in soil moisture are explored. Crist et al. (1984) used a spectrophotometer to measure reflectance at various soil moisture contents of several soil types. They found that a consistent relationship existed between soil moisture content and TM bands 5 and 7. Crist et al. (1984) states that:

> "The overall shape of the moisture/reflectance curves is fairly similar for the various soils. However, consistent with previous findings, there is significant difference between soils. Darker soils like Brookston exhibit low reflectance even at low moisture content, while other soils exhibit much higher reflectance at the same moisture levels. Thus while the basic relationship between soil reflectance and soil moisture suggests that reflectance could be

TM SPECTRAL BANDS
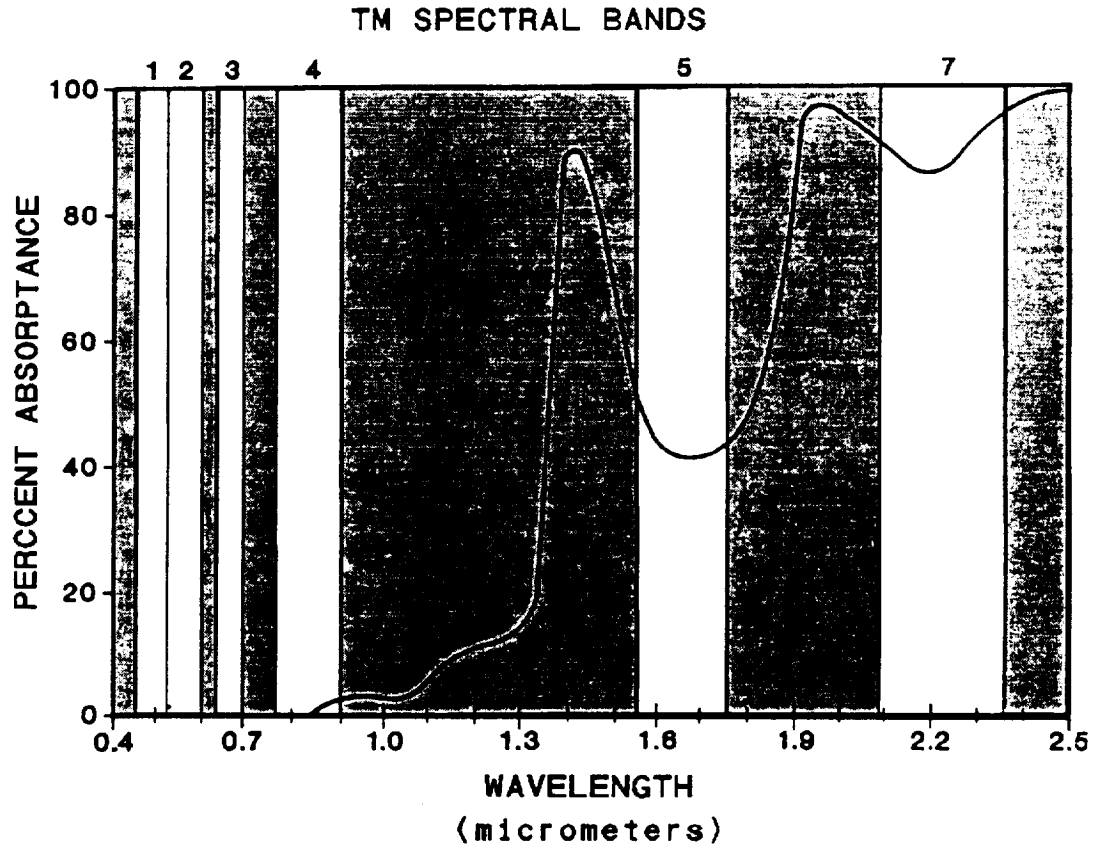
Figure 2. Water absorbance superimposed on the Thematic
Mapper bands (modified from Bunnik (1978)).

effectively used to measure the water content of
soils, such an approach could only be used for
soils whose general reflectance characteristics
were already know."

Reflectance curves of the six reflective TM bands at
different soil moisture contents, for a particular soil
type, are shown in Figure 3. This figure illustrates the
overall increase in reflectance as the soil becomes drier.
Soil moisture content was measured in percent of the weight
of the oven dried sample (Crist et al., 1984). As can be
seen in Figure 3, bands 5 and 7 are most sensitive to
changes in moisture content. Crist et al. (1984) found that
this relationship is consistent over several types of soil,
with textures ranging from clayey to sandy.

2.4 Feature Extraction

Features which are important to this study are
concerned with physical features of the terrain influencing
reflectance, as described in section 1.4, and image
features inherent in the TM data. Image features can be
separated into two catagories: spectral features and
statistical features.

2.4.1 Spectral feature extraction.

Spectral features are directly related to physical
features of the terrain; they result from and are highly
influenced by the most prominent characteristics of the

TM SPECTRAL BANDS
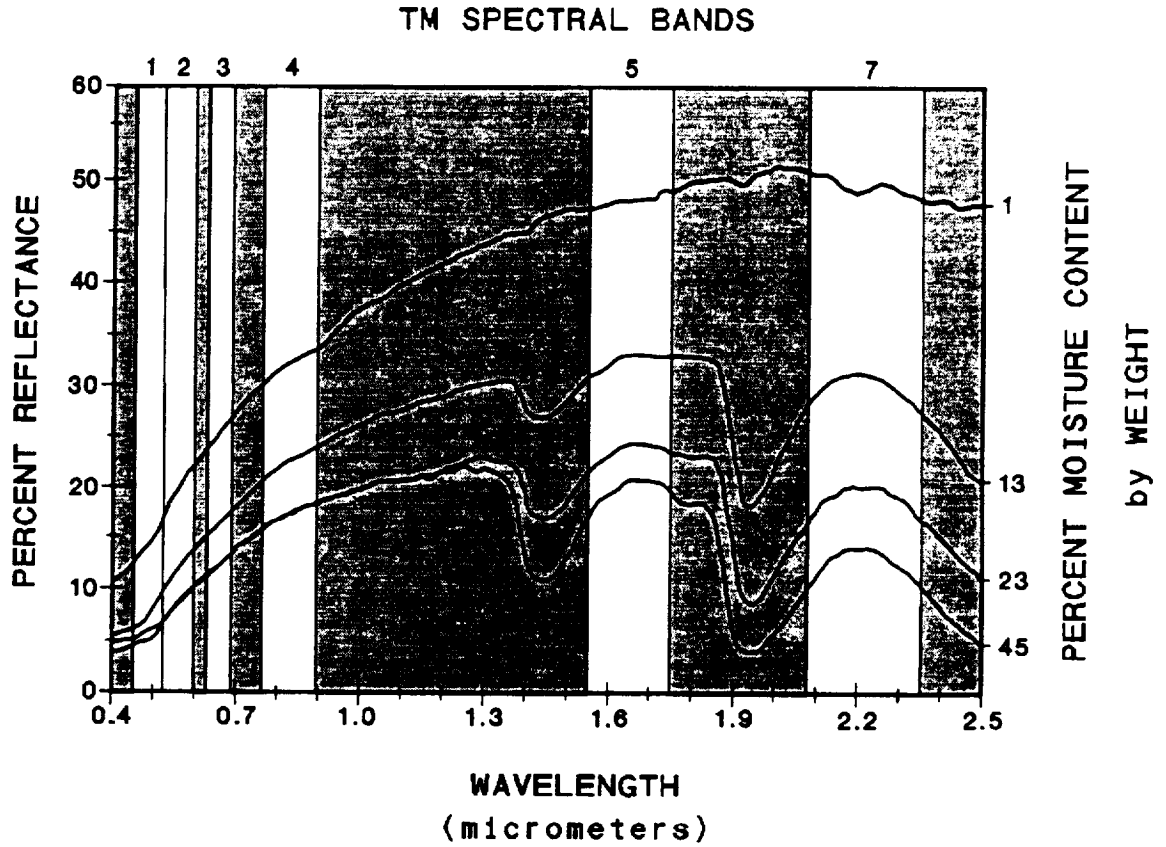
Figure 3. Soil reflectance curves at different soil moisture
contents, superimposed on the Thematic Mapper bands
(after Crist et. al 1984).

terrain. Some very prominent spectral features are bright soil, dense vigorous vegetation, and water.

A transformation developed by Kauth and Thomas (1976) called the "Tasseled Cap Transformation", can be used to extract the spectral features of brightness and greenness from MSS data; brightness being related to the physical characteristics of soil and greenness being related to the physical characteristics of vegetation. The term "Tasseled Cap" refers to the pattern of data points, plotted on a graph, that have been sampled from the pixels of an MSS image transformed into brightness and greenness. The tasseled cap shape results from the reflectance characteristics of soil and vegetation.

Crist and Cicone (1984c) describe a physically-based transformation of TM data developed from the Kauth and Thomas (1976) Tasselled Cap transformation. The Crist and Cicone (1984c) physically-based transformation was developed specifically for use with the six reflective bands of TM data. In Crist and Cicone (1984c) the TM tasselled cap transformation was found to result from physical features of the terrain. The three primary physical features are: brightness, greenness, and wetness. Wetness is a new feature not available from MSS data.

There are many other techniques described and tested in the literature for identifying physical features in remote sensing data (Richardson and Wiegand, 1977; Perry

and Lautenschlager, 1984; and Elvidge and Lyon 1985). Several researchers (Prost, 1980; Sadowski and Abrams, 1983; and Podwysoki et al., 1983) have demonstrated that a ratio of multispectral data in the spectral regions of TM bands 5 to 7 indicate the physical features of hydrothermally altered rock and soil with high concentrations of hydroxyl-bearing minerals, such as clay or alunite.

Band ratios were tested and evaluated as part of this research. Two band ratios were selected for further analysis because they are representative of the information content of the TM data used in the study. The first, a ratio of band 3 to band 7 (3/7) was calculated and then expanded to the full data range of 0 to 255 using a natural logarithmic function. The second ratio is a band 5 to band 7 (5/7), this ratio was expanded to the full range using a simple linear function. Both of the above band ratios were inverted by subtracting the resulting pixel value of the band ratio from 255 to maintain a positive relation with the topography. Spectral extraction techniques, such as the Tasselled Cap Transformation and the TM band ratios, are able to provide a quantitative indication of terrain characteristics through the physical interaction of electromagnetic radiation with terrain elements. However, the interaction between the spectral reflectance and the terrain must be studied to determine how the results of

each image feature extraction technique is linked to the physical features of the terrain.

2.4.2 Statistical Features.

Statistical algorithms implemented on computers attempt to emulate human interpretation of imagery. Human interpretation of remote sensing imagery would rely heavily on the textural and tonal variation to identify terrain features. Haralick et al. (1973) describes the concept of tone and texture as follows:

> "...tone is based on the varying shades of gray resolution cells [pixels] in an image, while texture is concerned with the spatial (statistical) distribution, of gray tones."

One example of a statistical feature that can be extracted from digital remote sensing imagery is texture. Texture and tone are used to define pattern, from which terrain features are identified. A comparative study of statistical techniques used to measure image texture for terrain classification, using MSS imagery, is presented in Weszka et al. (1976). In Weszka et al. (1976) several algorithms are tested, such as angular second moment, contrast, correlation, inverse difference moment, and entropy. All of these procedures where tested at all sampling angles within a window of pixels from an MSS image. Weszka et al. (1976) concluded that the statistical feature of angular second moment, when added to the pattern recognition procedure, yielded a results that improved the recognition of cover types over other techniques.

Image filters were also tested to determine possible presence of noise, or variation in the TM data not related to features of the terrain. Some effects of noise can by removed from digital imagery using filters that smooth the data by averaging a pixel value over a its neighboring, surrounding pixels. A filter such as this, can be used to remove the grainy appearance in some digital imagery. This type of filter replaces the value of a pixel with the average of its neighbors if its value deviates considerable from the surrounding pixels. ELAS, the software system used in this study, has an image filter called FLSIFT. This filter is described by Graham et al. (1980) as follows:

> In generating the output, the same operation is repeated for each pixel. The operation is performed with a 7 line by 7 column window or matrix with the output pixel corresponding to the center of the window receiving the results of the operation. The process starts by clustering the center pixel (location 4,4) with the pixel adjacent to it that has a minimum distance in n-space, where n is the number of input data channels, from the center pixel. Each additional pixel clustered is chosen from all the pixels adjacent to any of the previously clustered pixels. The pixel chosen to be clustered is the one with the minimum summation of the distances from the cluster mean in each channel. This pixel clustering continues until N pixels have been clustered. N is an input option within the range of 3 to 20. At the completion of the clustering, two output channels are written for each input channel processed. One contains the mean of the cluster and the other contains the standard deviation multiplied by eight.

Any of the possible channels of mean cluster values, and standard deviations of the clusters, can be selected for output.

Another example of statistical feature extraction is trend surface analysis. Trend surface analysis is a method of separating the data from a TM band into two components. The first component is the trend of the reflective surface, computed as a linear function of the TM image coordinates. The trend surface is the regional trend of the surface, the general shape of the reflective surface with local variations removed. The second component is the residual surface, which contains the local fluctuations in the reflectance surface with the regional variations removed. The linear function to be applied to the data must minimize the squared deviations from the trend of the surface (Davis, 1973). By minimizing the squared deviation of the trend, the resulting residual surface gives the best approximation of the local variability. The ELAS program called TREN was used for the trend surface analysis in this research. The TM data were modeled with TREN by a polynomial equation using the least squares technique as a "TREND SURFACE" (Gramham et al. 1980). A maximum tenth order trend surface can be modeled with TREN.

CHAPTER 3

AERIAL PROFILING of TERRAIN SYSTEM DATA PROCESSING

3.1 Introduction

The Aerial Profiling of Terrain System (APTS) is an experimental airborne inertial surveying system, supplemented with laser instruments which provide measurements of ground position and elevation. Designed to be carried on relatively small aircraft, the APTS was installed on a De Havilland Twin Otter aircraft to survey the GSLD. APTS consists of a inertial measurement unit, a laser tracker, a laser profiler, a computer system, and a video camera and recorder. Figure 4 represents the APTS in use over the GSLD. During data collection the laser tracker provides positional information used to reference the profile data to the local datum.

The APTS requires the use of geodetic control in the form of surveyed points on the ground where retroreflectors are mounted. The laser tracker uses the retroreflectors to measure ranges and angles from the APTS to the geodetic control points. The geodetic control points used in the survey of the GSLD consist of either surveyed Section or Township corners or geodetic benchmarks. These points form
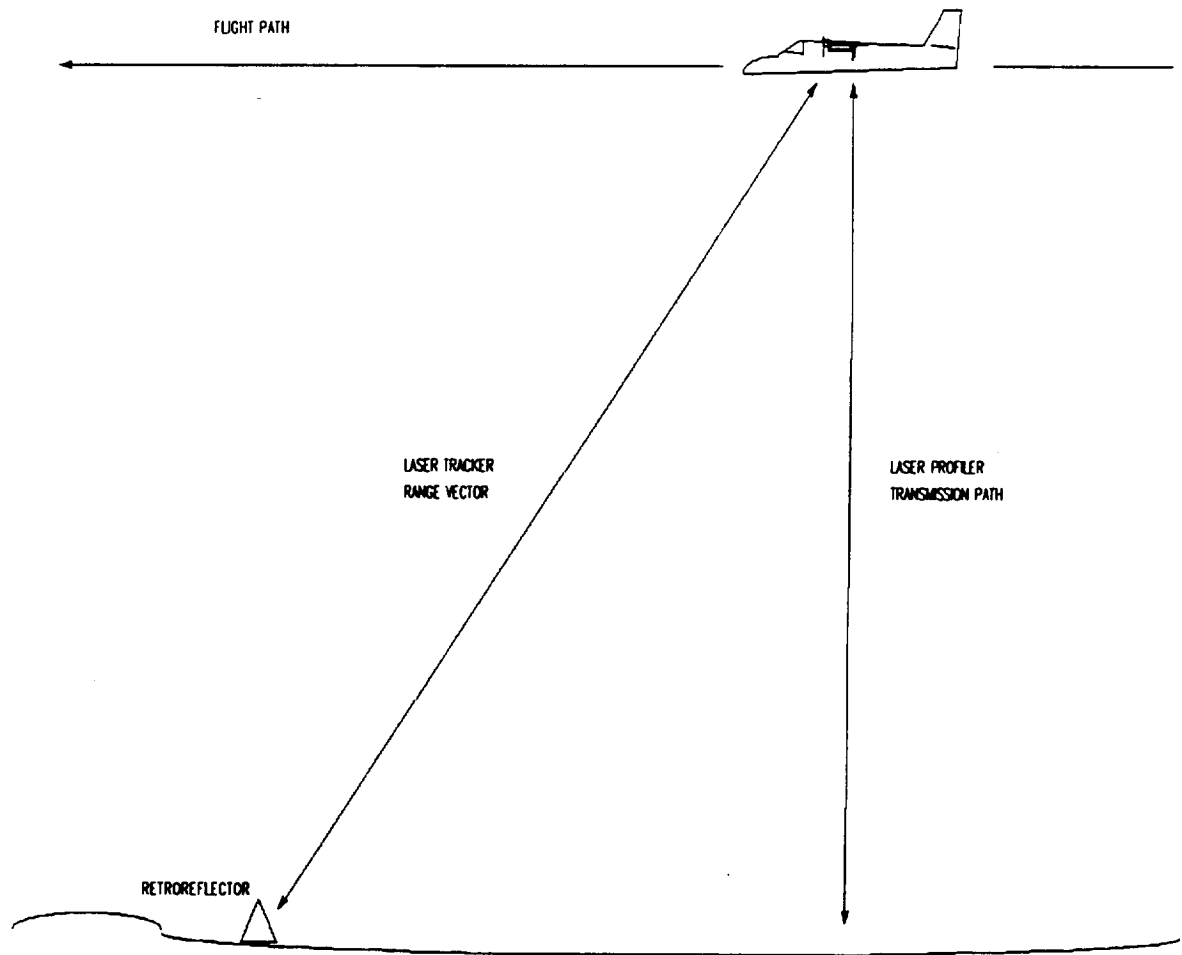
Figure 4. Aerial Profiling of Terrain System (APTS) (modified from Cyran (1983)).

a grid, spaced about 9.7 kilometers (6 miles) apart with accurate elevations available for most points. Grid spacing of 9.7 kilometers (6 miles) provides approximately 180 seconds of flying time between retroreflectors when flying at 100 knots along a grid line. If the APTS successfully finds retroreflectors within 200 seconds the vertical accuracy can be as close as ± 15 cm (1/2 foot) with a horizontal accuracy of ± 61 cm (2 feet), while flying at a height of 488 meters (1600 feet) above the mean ground level at 100 knots. However, the flight time between retroreflectors on the diagonal is about 4.5 minutes (Donna 1985; Chapman 1985; Cyran 1983). Figure 5 shows the pattern of the APTS survey of the GSLD.

While data collection is in progress the on-board computer provides the cockpit of the aircraft with navigation information, displaying heading, deviation angle, and distance from the last retroreflector. Navigation is accomplished by applying measurements made by the laser tracker which include the range and two angles from the APTS to the retroreflector. As the aircraft approaches a retroreflector the computer directs the laser tracker to begin looking for it. The laser tracker uses a spiral search pattern around the computed location until a return is obtained from the retroreflector. When a return is obtained the laser tracker locks on to the position of the retroreflector and measurements of range and direction
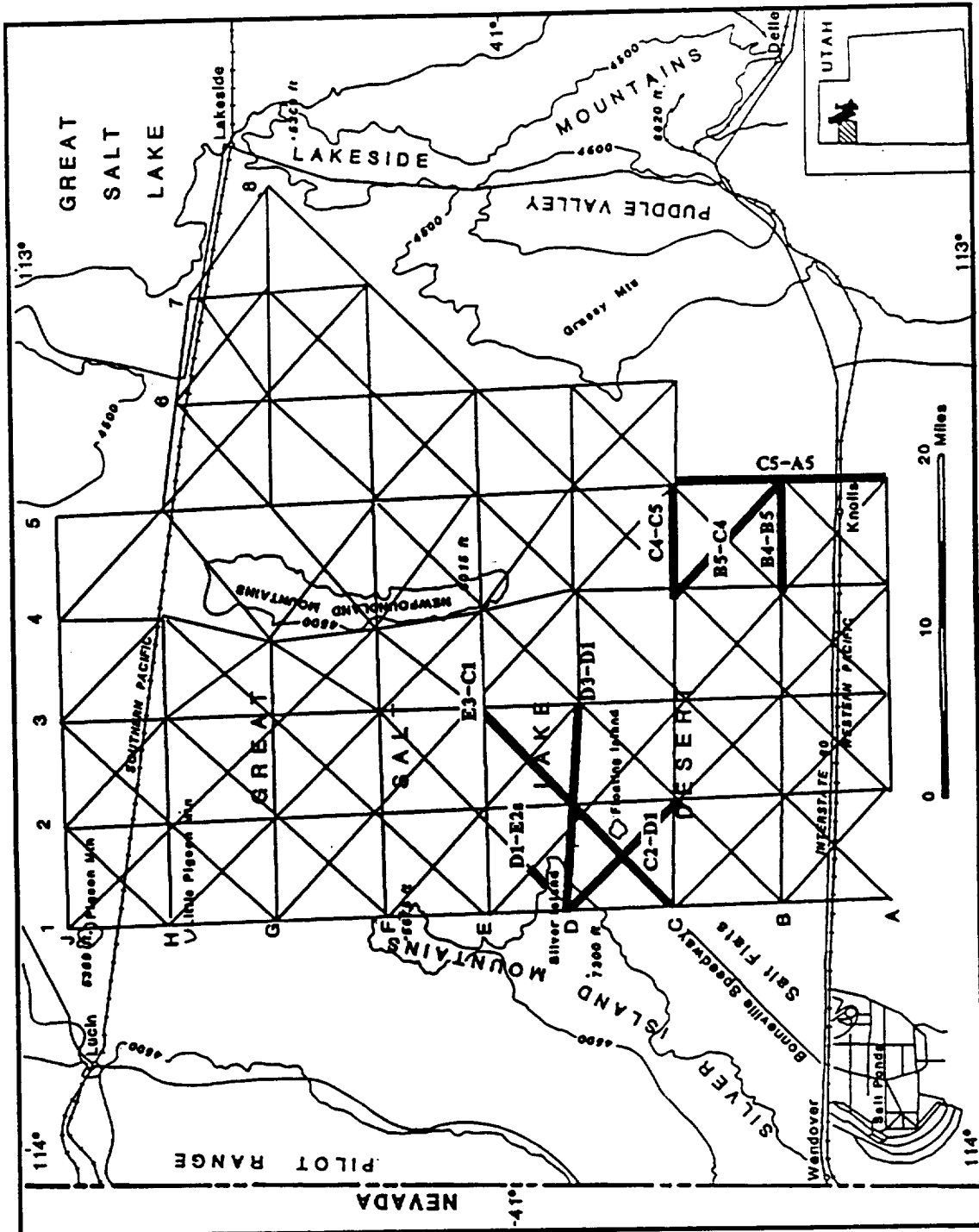
Figure 5.   Pattern of the APTS survey of the GSLD.

are made automaticly until the vertical angle of the APTS to the retroreflector reaches 60 degrees. Each time the laser tracker locks-on to a retroreflector, the updated positional information is used to reset the navigated position (Chapman 1985; Cyran 1983).

The APTS laser profiler measures the distance between the aircraft and the terrain below. Distances are determined by measuring the time differences between transmitted and received laser pulses. After the mission has been completed, the APTS data are processed by a mainframe computer with software to edit, correct the X,Y position of points, compress, filter, smooth, and recombine the data into a survey data set.

3.2 Merging Profile Data with TM Data

The APTS survey data, which is the final product of the APTS survey, consists of five entries for each profile point. Table 2 displays a sample survey data set that corresponds to one TM pixel. The first entry in Table 2 is the mission number, the second is the time the point was recorded, the third is the latitude, the fourth is the longitude, and the fifth is the elevation in feet. Merging of the data begins with transforming the latitude and longitude to Universal Transverse Mercator (UTM) coordinates.

TABLE 2

SAMPLE OF THE APTS SURVEY DATA SET FOR ONE PIXEL.

POINT	MISSION NUMBER	APTS TIME (0.01 sec)	LATITUDE	LONGITUDE	ELEVATION (ft)
1	85080101	15772294	40 58 25.0794	113 39 51.9489	4228.54
2	85080101	15772298	40 58 25.1395	113 39 51.8868	4228.31
3	85080101	15772302	40 58 25.1976	113 39 51.8207	4227.64
4	85080101	15772306	40 58 25.2538	113 39 51.7513	4227.26
5	85080101	15772310	40 58 25.3091	113 39 51.6806	4226.49
6	85080101	15772314	40 58 25.3630	113 39 51.6075	4225.88
7	85080101	15772318	40 58 25.4174	113 39 51.5361	4225.44
8	85080101	15772322	40 58 25.4718	113 39 51.4651	4224.90
9	85080101	15772326	40 58 25.5268	113 39 51.3955	4224.54
10	85080101	15772330	40 58 25.5818	113 39 51.3266	4224.42
11	85080101	15772334	40 58 25.6391	113 39 51.2612	4225.01
12	85080101	15772338	40 58 25.6987	113 39 51.1990	4225.65
13	85080101	15772342	40 58 25.7583	113 39 51.1355	4225.16
14	85080101	15772346	40 58 25.8181	113 39 51.0719	4224.51

With the UTM coordinates for each profile point, it is possible to determine the TM pixel that a profile point falls within. Determining which pixel a profile point falls within involves converting the UTM coordinate for the profile point into TM coordinates. This is done by using the coefficients derived from the geographic referencing of the TM image data, described in Section 2.2. The geographic referencing coefficients allow one to transform the TM coordinates, line (Y) and element (X) of the center of a pixel, to UTM coordinates, northing (Y) and easting (X), or from UTM coordinates to TM coordinates. Table 3 is a sample of the APTS profile points, that fall within the same pixel as in Table 2, and have been transformed into UTM coordinates and then TM pixel coordinates.

The APTS profiler collects profile points approximately every 1.5 meters (5 feet) (Mamon et al. 1978). At this rate of data collection there is a possibility of 20 points falling within a TM pixel in the line (Y) or element (X) direction. However, across the diagonal of a pixel there could be as many as 28 points. Analysis of the APTS data for the GSLD shows that there are fewer than 20 points in all of the pixels processed and an average of 14 points per pixel. This indicates a data collection rate less than is indicated in Mamon et al., 1978. The data collection rate is closer to a two-meter interval between points in the GSLD survey.

TABLE 3

SAMPLE COORDINATE OF APTS DATA FOR A PIXEL

POINT	EASTING	NORTHING	ELEMENT	LINE	ELEVATION (FT)
1	275810.56	4539037.64	2675.50	600.78	4228.54
2	275812.07	4539039.44	2675.68	600.41	4228.31
3	275813.67	4539041.19	2675.72	600.34	4227.64
4	275815.34	4539042.87	2675.77	600.27	4227.26
5	275817.05	4539044.53	2675.81	600.20	4226.49
6	275818.81	4539046.14	2675.86	600.13	4225.88
7	275820.53	4539047.76	2675.91	600.06	4225.44
8	275822.24	4539049.39	2675.96	599.99	4224.90
9	275823.92	4539051.04	2676.00	599.92	4224.54
10	275825.58	4539052.69	2676.05	599.86	4224.42
11	275827.16	4539054.41	2676.09	599.78	4225.01
12	275828.67	4539056.20	2676.13	599.71	4225.65
13	275830.21	4539057.99	2676.17	599.64	4225.16
14	275831.75	4539059.79	2676.20	599.57	4224.51

These sample coordinates are from the APTS data for the pixel shown in Table 2. The coordinates are transformated from latatude and longitude to Universal Transferse Macator (UTM) and then to TM Line and Element.

3.3 Profile Statistics for Each Pixel

Statistical processing of the APTS data was necessary in order to allow for the comparison of no less than 10 APTS profile points to one TM pixel. To insure correct representation of elevation, pixels with less than 10 points were excluded from analysis. Elevations for the profile points from the data in Tables 2 and 3 are shown in Figure 6. Figure 6 is representative of the amount of variability that can occur within a pixel. The following is a list of the descriptive statistics that were calculated in order to access how well the average elevation for each pixel represented the terrain:

    Mean Elevation
    Standard Deviation
    Variance
    Median
    Minimum
    Maximum
    Range
    Coefficient of Variation
    Skewness

Table 4 shows a sample output from the descriptive statistics program, called LASER, developed for this study. The statistics on the first line in Table 4 are from the pixel in Table 3. Relief ratio, percent ridge, and percent trough were calculated in order to attempt to find a parameter that described the terrain configuration in a given pixel. The standard deviation, variance, minimum,
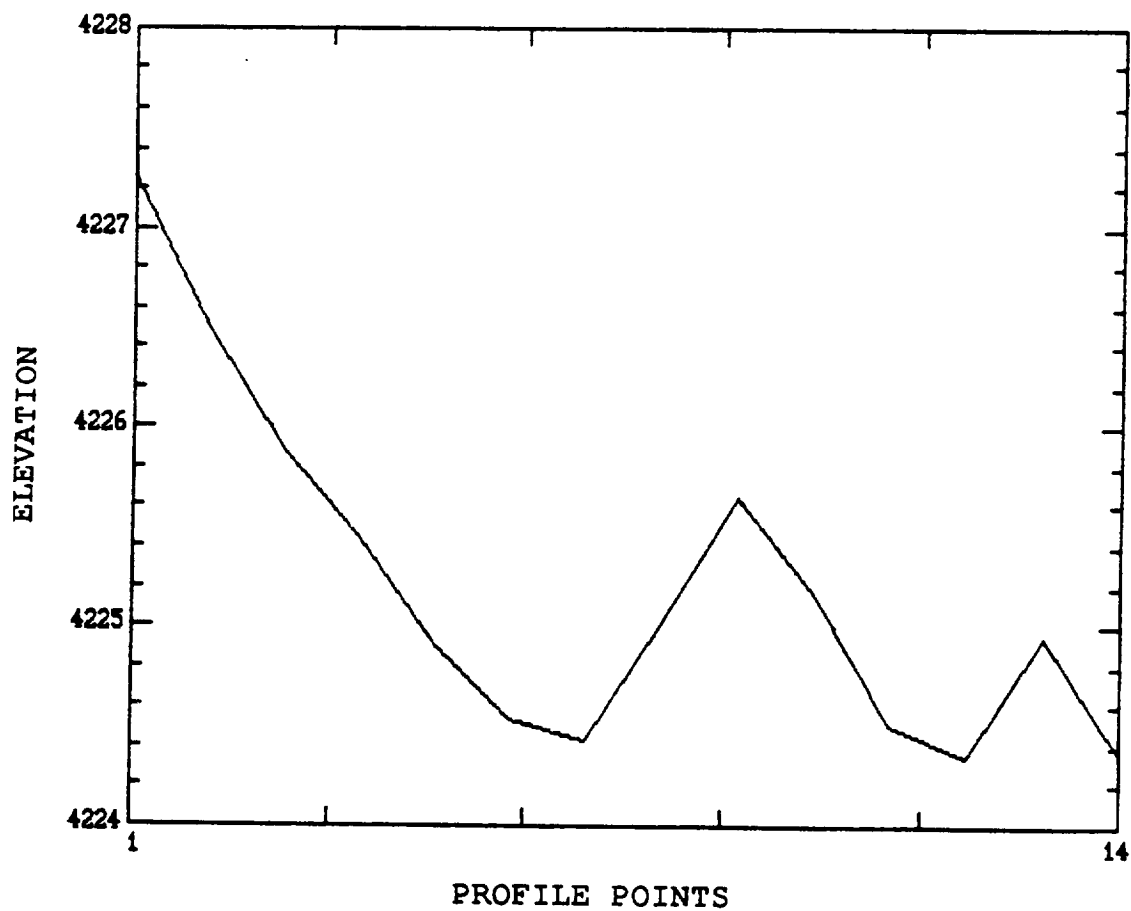
Figure 6. Plot of the profile points from the pixel in Table 3.

TABLE 4

SAMPLE OF THE DESCRIPTIVE STATISTICS FROM APTS SURVEY DATA.

Element	Line	Median	Average	SD	Variance	COV	Maximum	Minimum	Range	Skew	RR	%R	%T	N
2676	600	4225.54	4225.98	1.4275	2.0378	0.0338	4228.54	4224.42	4.12	-0.44	0.0735	50	36	14
2677	598	4228.32	4227.82	1.4354	2.0603	0.0340	4229.18	4225.02	4.16	0.50	0.1038	29	50	14
2678	596	4222.50	4222.54	0.1536	0.0236	0.0036	4223.00	4222.39	0.61	-0.04	0.0116	0	0	13
2678	595	4222.40	4222.38	0.0700	0.0049	0.0017	4222.48	4222.22	0.26	0.02	0.0027	0	0	13
2679	594	4222.13	4222.29	0.3814	0.1455	0.0090	4223.11	4221.97	1.14	-0.16	0.0305	0	20	10
2679	593	4221.79	4221.87	0.1725	0.0298	0.0041	4222.25	4221.69	0.56	-0.07	0.0063	0	0	14
2679	592	4221.65	4221.66	0.1216	0.0148	0.0029	4221.85	4221.45	0.40	-0.01	0.0126	0	0	12
2680	591	4221.62	4221.61	0.0928	0.0086	0.0022	4221.74	4221.44	0.30	0.02	0.0060	0	0	10
2681	590	4226.64	4226.13	2.2495	5.0603	0.0532	4228.45	4222.01	6.44	0.51	0.0806	31	50	16
2682	588	4227.62	4227.40	0.5070	0.2570	0.0120	4227.92	4226.23	1.69	0.22	0.0035	14	7	14
2682	587	4224.33	4224.20	1.0710	1.1471	0.0254	4226.12	4222.77	3.35	0.13	0.0526	36	29	14
2683	586	4220.78	4220.50	1.5100	2.2801	0.0358	4222.26	4218.29	3.97	0.28	0.0414	42	50	12
2684	585	4217.98	4218.02	0.1678	0.0281	0.0040	4218.25	4217.80	0.45	-0.04	0.0138	0	0	13
2684	583	4217.22	4217.21	0.1208	0.0146	0.0029	4217.39	4216.97	0.42	0.01	0.0002	0	0	15
2685	582	4216.78	4216.81	0.0620	0.0038	0.0015	4216.89	4216.71	0.18	-0.03	0.0025	0	0	10
2686	581	4216.61	4216.60	0.0897	0.0081	0.0021	4216.80	4216.46	0.34	0.01	0.0048	0	0	13
2685	580	4216.78	4216.74	0.1440	0.0207	0.0034	4216.93	4216.54	0.39	0.04	0.0073	0	0	15
2686	578	4216.84	4216.84	0.0811	0.0066	0.0019	4216.99	4216.67	0.32	0.00	0.0075	0	0	11

SD = Standard Deviation
COV = Coefficeint of Variation
RR = Relief Ratio
%R = Percent Ridge
%T = Percent Trough
N = Number of Profile Points in this Pixel

maximum, and the coefficient of variation provides a measure of the variability of relief at the sub-pixel level. While the median, mean, and skewness provide a measure of the distribution of relief within the pixel. The relief ratio is calculated by dividing the elevation difference, in meters, for a pixel, by the distance, in meters, between the first point and the last point in the pixel. Relief ratio is used to approximate the relief over the length of the pixel. Percent ridge is defined as the number of points with elevation values that exceed the mean pixel elevation by more than 15 cm (1/2 foot) divided by the number of points for the pixel multiplied by 100. Percent trough similarly, is the number of points with elevation that are less than the mean pixel elevation by more than 15 cm divided by the number of points for the pixel multiplied by 100. Values of percent ridge and trough are calculated because the ridges were expected to have higher reflectance than the troughs due to soil moisture differences. Selected profile statistics, calculated from the APTS points per pixel, for a sample of 36 pixels from profile D1-E2 (D1-E2s) are shown in Figures 7, 8, and 9. Figure 7 is the mean elevation for each of the 36 pixels, Figure 8 is the standard deviation and Figure 9 is the relief ratio.
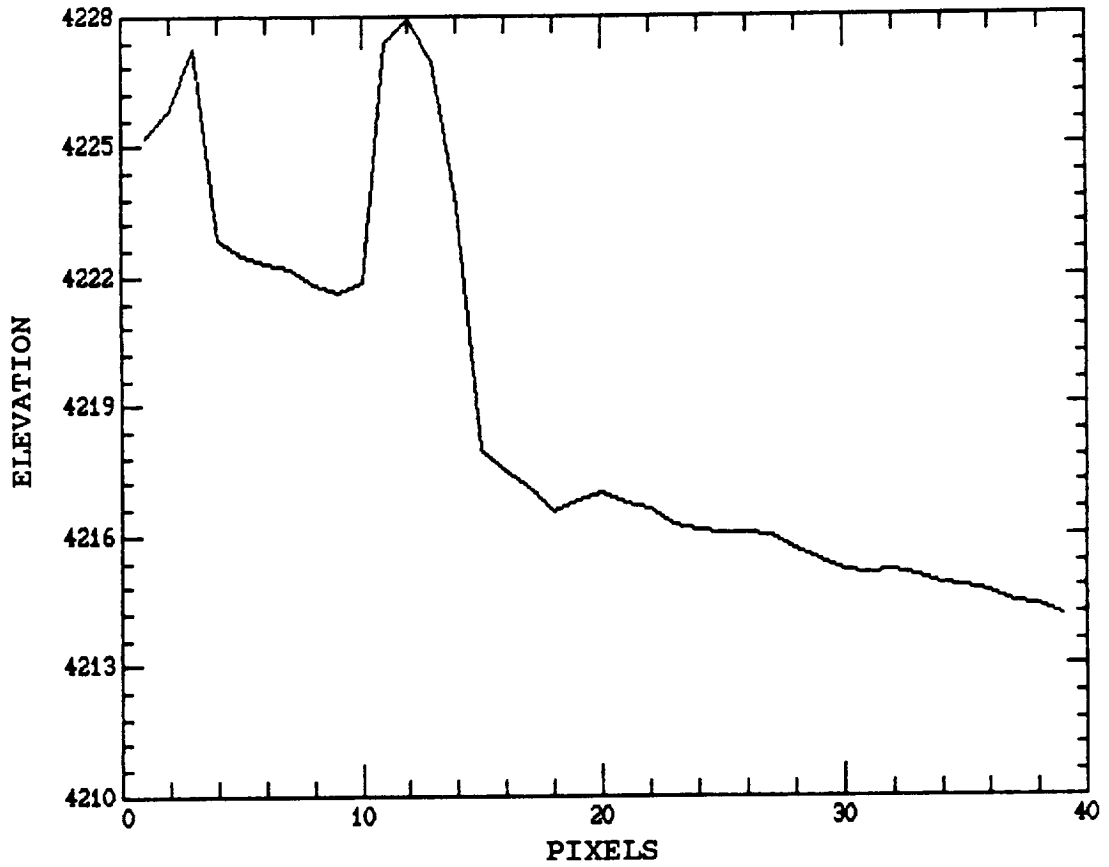
Figure 7. Plot of mean pixel elevations, mean calculated from
the APTS points per pixel, for 36 pixels from profile
D1-E2s.
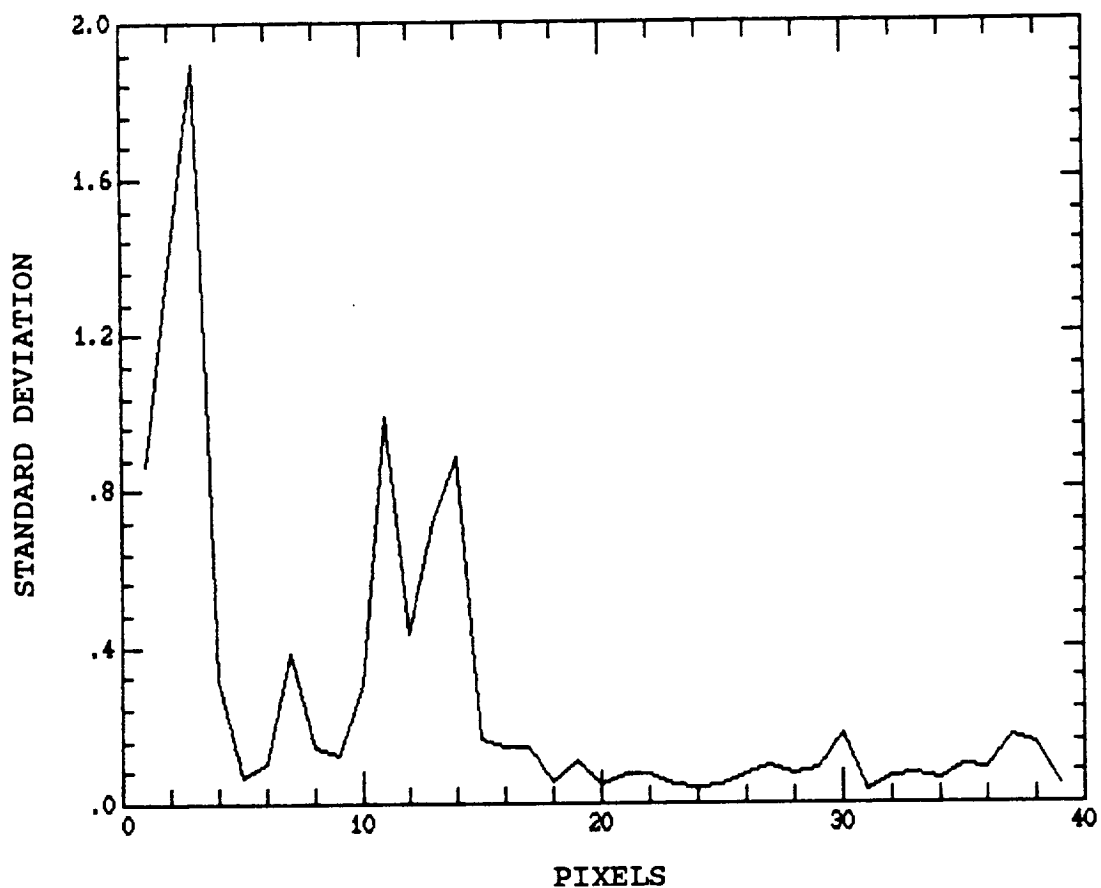
Figure 8. Plot of standard deviation, ccalculated from the APTS
points per pixel, for 36 pixels from profile D1-E2s.
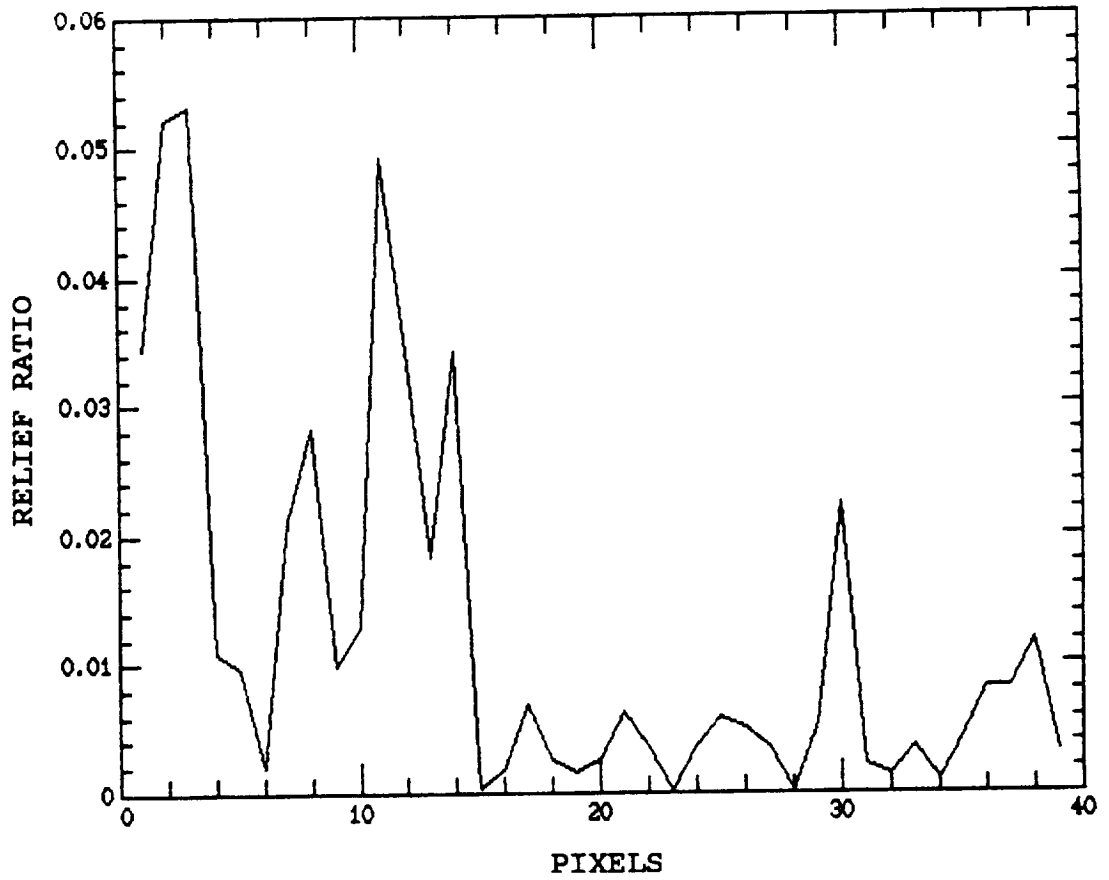
Figure 9. Plot of relief ratio, calculated from the APTS points
per pixel, for 36 pixels from profile D1-E2s.

CHAPTER 4

TERRAIN MODEL

4.1 Exploring the Data Structure

The purpose of exploring the spectral data structure
is to determine the information content in the TM imagery.
The structure is a result of the spatial distribution of
reflected light from the terrain as detected by the TM
scanner. The dimensions of the TM data include the X and Y
coordinates of each pixel as well as a Z coordinate (i.e.,
the digital value (DV) for each band of each pixel), which
gives the TM data 3 dimension in each of the bands. The
approach used for exploring the data structure follows that
of Kauth and Thomas (1976), as quoted in section 1.5. The
key element of this approach is the variety of ways the
data are displayed. Understanding of the data structure
often depends on the variety of displays used - one must be
able to visualize the data structure in order to formulate
a physical interpretation or a quantitative methodology for
the construction of a formal model.

Gray tone images of the individual bands, as Figures
10 and 11 illustrate, are one of the most fundamental
displays used. Shown in Figure 12 are reference map for
Figures 10 and 11. These displays are very useful in
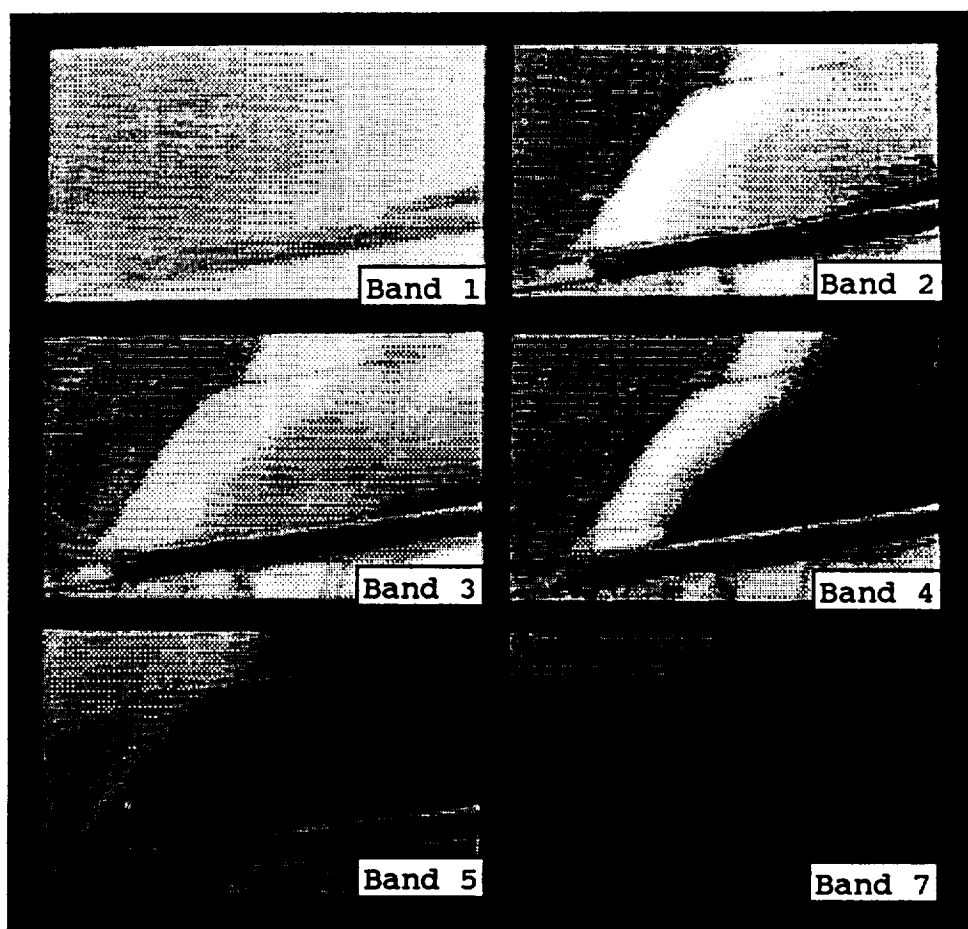
Figure 10. Gray tone images of the six reflective TM bands, July 2, 1984, over the Bonneville Salt Flats.
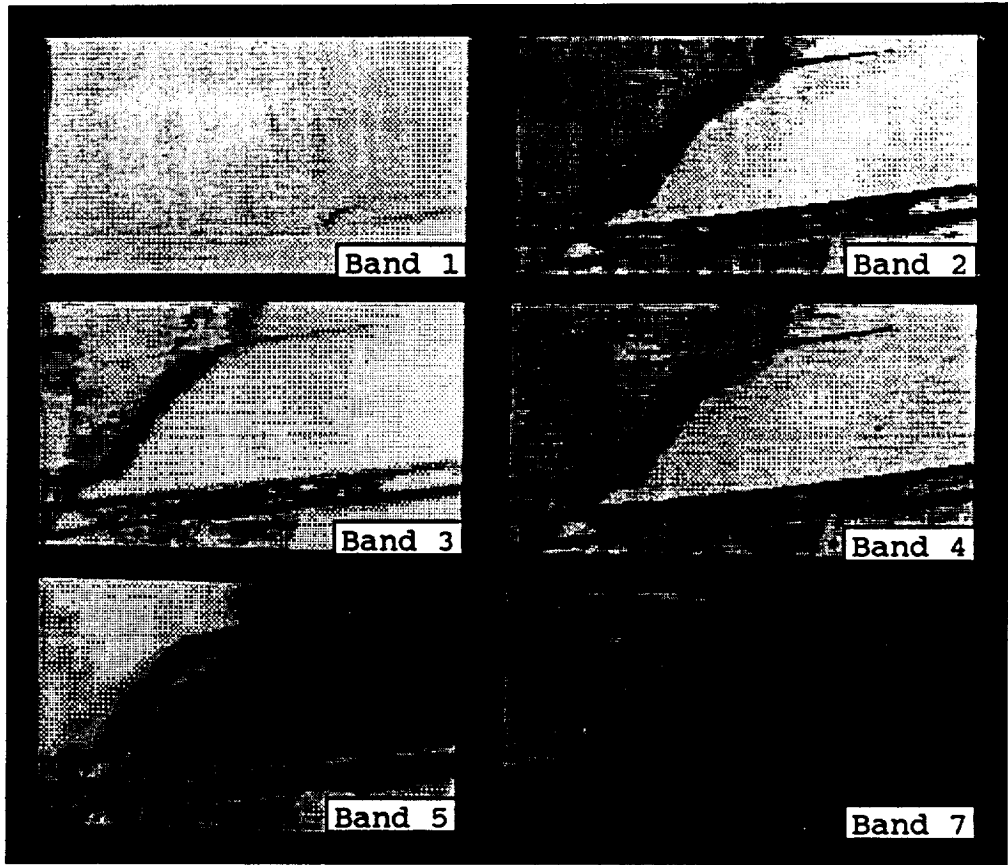
Figure 11. Gray tone images of the six reflective TM bands, June 19, 1985, over the Bonneville Salt Flats.
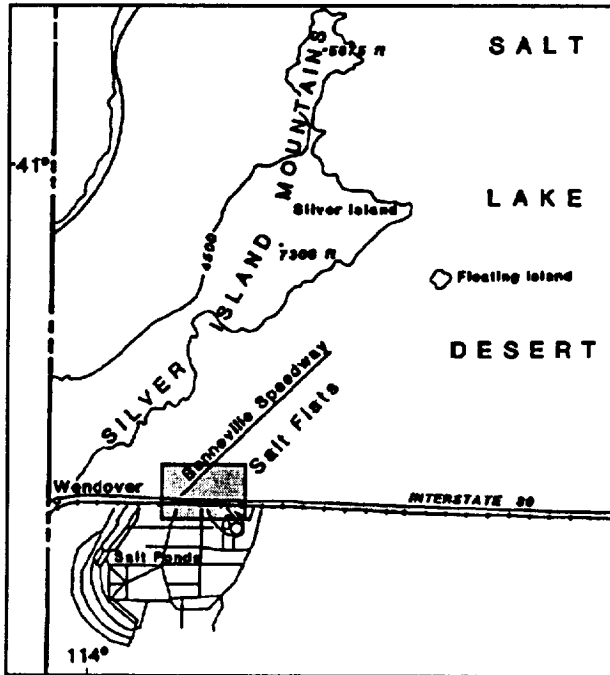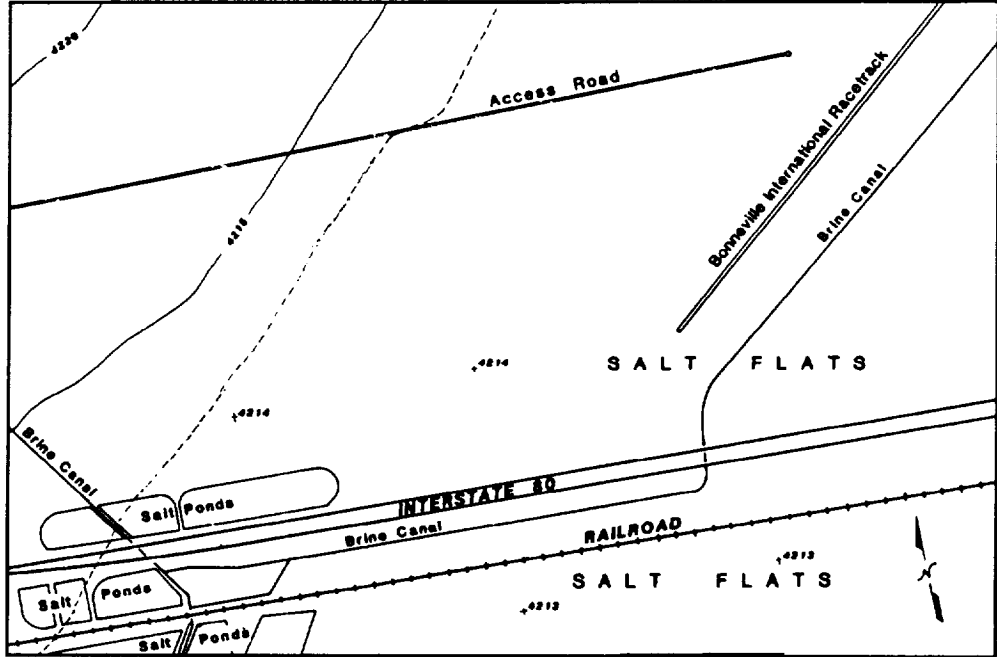
Figure 12. Reference maps of the Bonneville Salt Flats for the
TM images in Figures 10 and 11.

determining the information content and the actual number of distinct spectral dimensions in the TM data. A distinct spectral dimension is an individual TM band that contains unique information that is not redundant with other bands. The number of distinct spectral dimensions are most often less than the number of bands. Information content is determined through analysis of individual spectral dimensions and by investigating the information content of composite spectral dimensions (e.g., an a analysis of multiple TM bands). Figures 10 and 11 show the six reflective bands over a portion of the Bonneville Salt Flats for the two dates of TM data used in this research. Band 6 is not shown due to the low spatial resolution, causing the appearance of a blurred image which restricts the identification of reference features. Figure 10 is from the July 2, 1984 Landsat 4 TM scene, and Figure 11 is from the June 19, 1985 Landsat 5 TM scene.

The information that begins to emerge when viewing Figures 10 and 11 is that the seemingly featureless GSLD is not without its own complexity. The widely varying gray tones representing the spectral response indicates a complicated interaction between the terrain and the reflected light. The influence of soil moisture on reflected light is clearly evident when comparing the two dates of imagery. In the 1984 TM image, Figure 10, the dark area located between Interstate Highway 80 and the

railroad, and just north of the highway, on the east side of the scene, is most likely standing water. In the 1985 TM image, Figure 11, there is most likely only a small amount of standing water just right of center, between the highway and the railroad, at the bend in the brine canal. The surface of the Bonneville Salt Flats is a very bright white salt crust (Utah Geological and Mineral Survey, Bulletin 116, 1980); however, the dark tones in Figures 10 and 11 are caused by the absorbtion of light energy, which is most likely a result of soil moisture at or near the surface of the salt flats. As Figures 2 and 3 illustrate, the longer wavelength bands (e.g., bands 5, and 7) have higher moisture absorbtion characteristics. Most likely, there was a greater amount of soil moisture at the surface in Figure 10 as opposed to Figure 11, hence the brighter tones of most bands in Figure 11. The relationship between the topography and reflected light is also evident from Figures 10 and 11 (see Figure 12 for topography) as the elevation of the topography increases, so does the intensity of the reflected light in mid-infrared bands (bands 5, and 7), while bands 2 and 3 have the opposite relationship to the topography, and bands 1 and 4 have no apparent relationship.

As with most remote sensing research involving satellite data, it was not possible to be in the field collecting data during the overpass of the satellite.

However, lacking the field data necessary for a conclusive explanation regarding the spectral variation between July 2, 1984 and June 19, 1985, in the GSLD, the following plausible explanation is presented: Most likely soil moisture is the major factor involved in the spectral distinction between the geomorphic features, that are higher than the basin-floor, above 1284.7 meters (4215 feet), and the basin-floor salt flats. Other factors, such as vegetation and soil color, can influence the spectral response of the terrain (e.g., when soil moisture is low, and soil color is dark, or when ground covered by vegetation is great enough to contribute to the spectral variation).

During the exploration of the data structure, a relationship between the terrain and band 6 was discovered. Although it was not possible to verify, it appears that there is a thermal gradient between the basin-floor and the geomorphic features of the GSLD. Band 6 of the July 2, 1984, TM image, indicates that the moist salt flats are cooler than the surfaces of the geomorphic features (e.g., the tops of sand dunes). The thermal gradient is indicated by the gradient in DV's of band 6 between the basin-floor and geomorphic features (i.e., the basin-floor has lower values than the geomorphic features).

Another display used to gain insight into the data structure is the scatter plot. Scatter plots of the digital

values for each TM reflective band combination were plotted, as shown in Appendix A. Figure 13 shows one of the scatter plots produced, this is a plot of band 3 and band 7. This plot was produced from a sample of 525 pixels from the July 2, 1984 TM image below an elevation of 1290m (4235 feet). The sample data for this plot including various representative features of the GSLD, such as salt flats and sand dunes.

Much information about reflected light from the GSLD is contained in Figure 13. Most of the data points in Figure 13 form into the general shape of a triangle. At point "A" of the triangle, at the right of the plot, are data points result from light dry soil. Dark dry soil is depicted at point "B" in the lower left of the triangle. Very bright soil that is also wet, as in the salt flats shown in Figure 10, is represented at point "C", in the upper left of the triangle. The points that form a line above point "C", in the upper left corner, are a result of soil that is very bright white and highly reflective in band 3, this soil is also very wet; therefore, absorbing band 7. This line is formed from data points in band 3 that have, or are very close to, the maximum value of 255 and contain some variation in band 7. The points in this line also have the lowest values of all points used for this plot in band 7.

Another type of display used to gain insight into the

The pixels in this corner are the
from the brightest and wettest soil
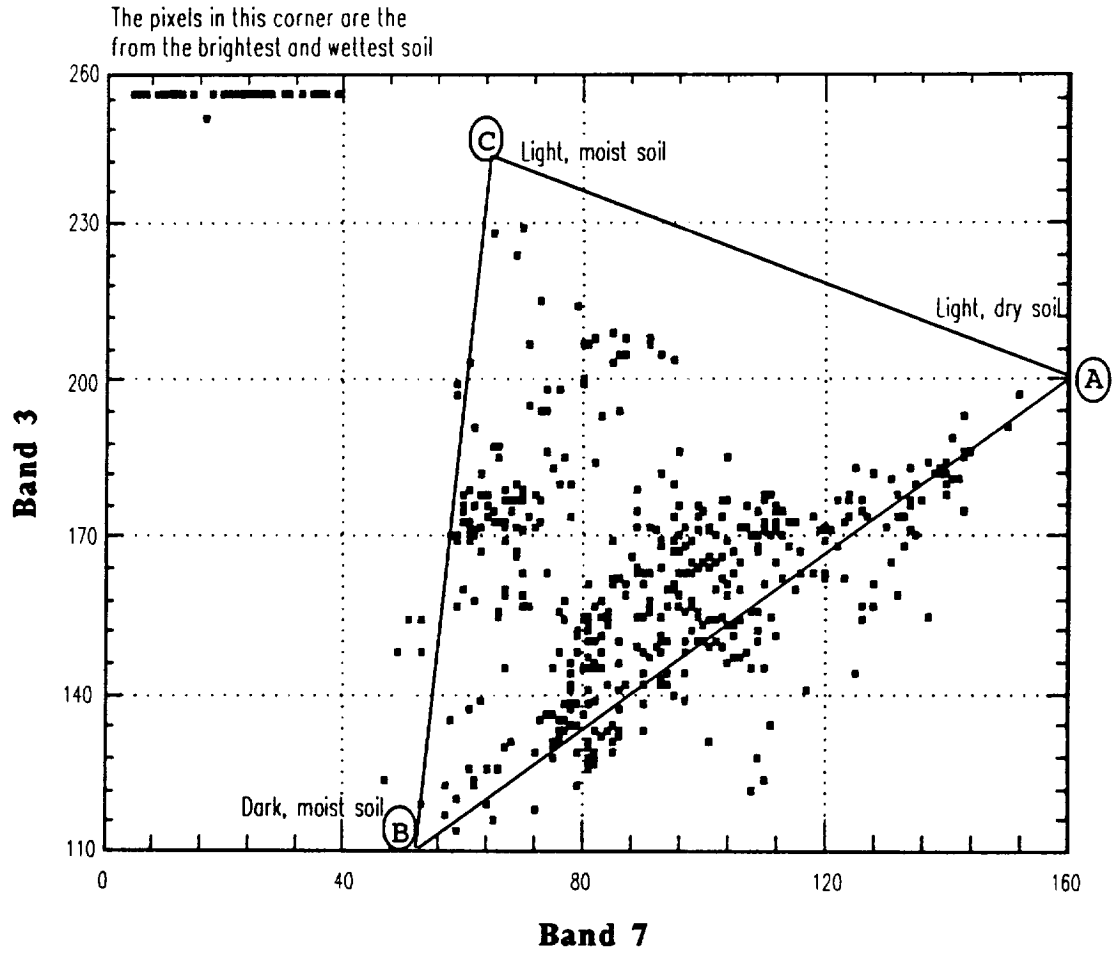
Figure 13. Scatter plot of TM band 3 and band 7, July 2, 1984.
525 pixels were sampled along APTS profiles from
representive features in the GSLD, such as salt flats

data is a plot of the digital values for each band along APTS profiles. Since, only relatively small portions TM data can be viewed in a two-dimensional line plot a three-dimensional perspective view of the reflectance surface or surface plot, as in Figure 14, was produced. Although the surface plot also covers a relatively small area, it provides a much greater insight into the data structure than other displays. The surface plot allow one to view the spatial character of the reflectance. This representation of the TM data lead to the hypothesis that a correlation must exist between band 7 and the morphometry of the terrain. This became the working hypothesis on which many subsequent samples were selected along APTS profiles throughout the study area.

Three-dimensional surface plots are also valuable for interpreting geomorphic features, such as terrain modified by lake-expansion. For instance, the trimline-like limit around the margins of sand dunes, caused by late Holocene expansion of the Great Salt Lake, is evident in Figure 14 (i.e. where the arrow is pointing). Superimposed on the surface plot in Figure 14 is the approximate location of the APTS profile D1-E2s. Figure 15 shows the two-dimensional line plot of the APTS profile, D1-E2s, over the pixels from Figure 14, with the trimline limit identified. Figures 7, 8, and 9 are produced from the same data, profile D1-E2s.
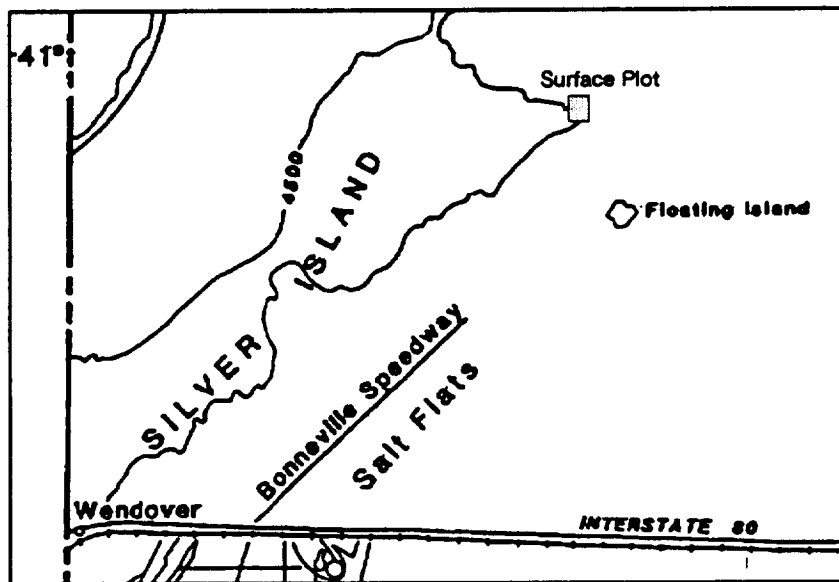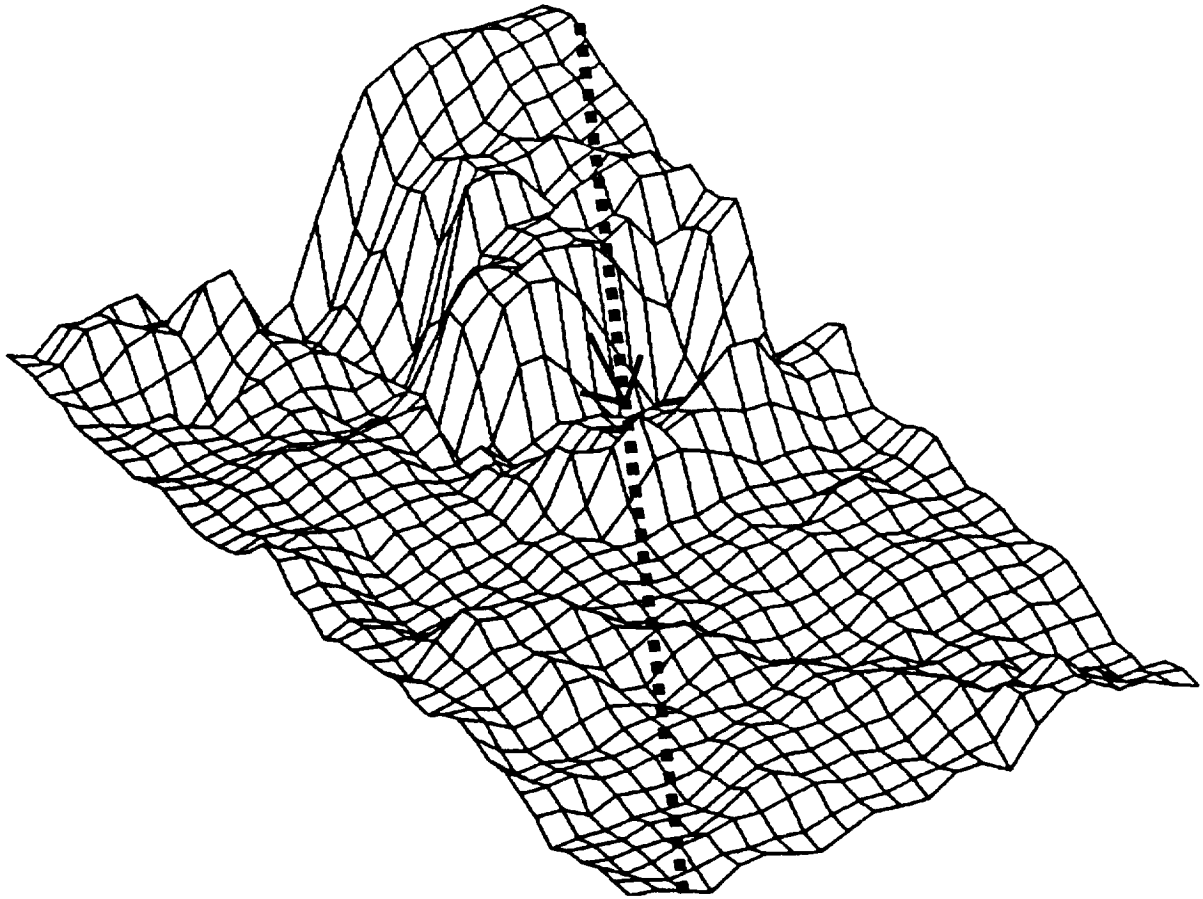
Figure 14. A three-dimensional surface plot, representing band
7 data, July 2, 1985. The heavy dashed diagonal line
represents a trace of the APTS profile D1-E2s. The
arrow points to the trimline.
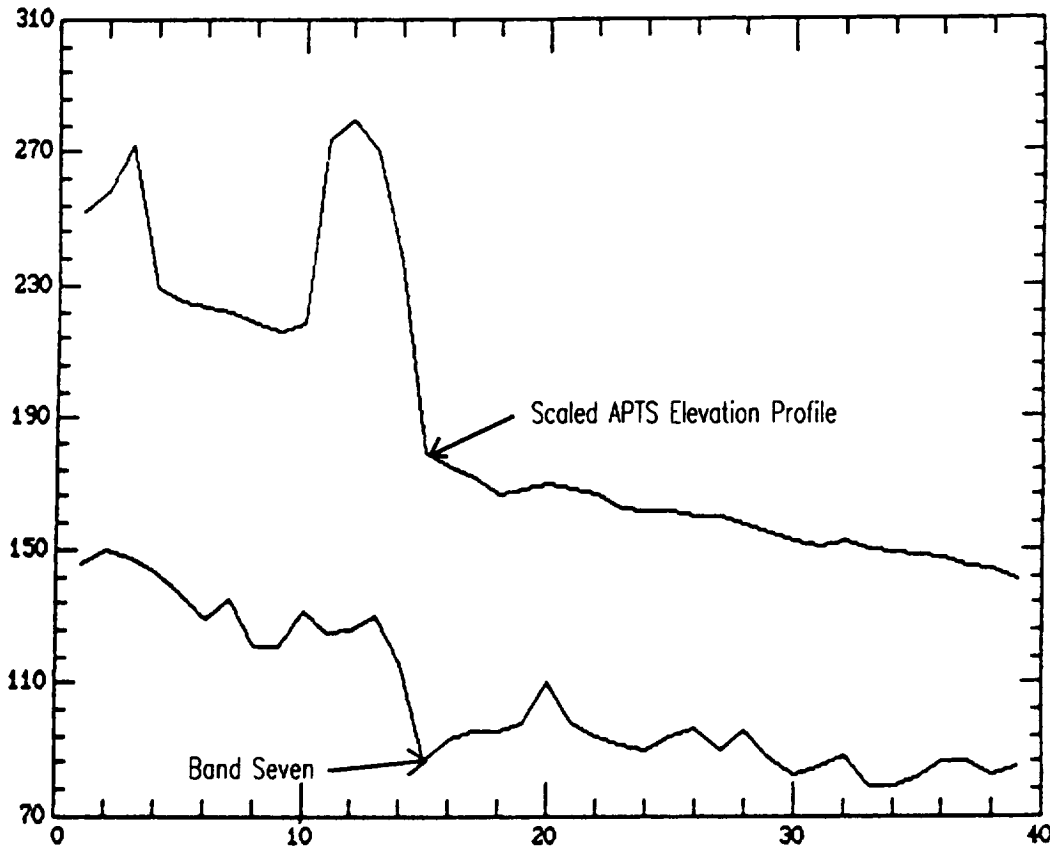
Figure 15. Two-dimensional line plot of band 7 and APTS profile
sample D1-E2s. Arrows point to the expression of the
trimline limit. The APTS mean pixel elevations have
been scaled to 0.1 feet per unit.

In addition to the foregoing spectral analysis, statistical analysis of the data was also used to gain insight into the data structure. Table 5 is a correlation matrix of the seven TM bands for the 1984 image. The correlation matrix provides a means of determining the information content in the data. Examination of Table 5 reveals that there is a high correlation between various spectral bands. It is evident that, apart from the thermal band 6, there appears to be only 2 strong spectral dimensions. The correlation matrix supports the results of the physical-based transformation, using Crist and Cicone (1984c) coefficients; the two spectral dimensions of the TM data over the GSLD are: brightness and wetness.

The spectral dimensions of the data were explored using physically-based transformations (e.g., Crist and Cicone (1984c)) and the scatter plots of each band combination. Physically-based transformations such as, Crist and Cicone (1984c), extract information about the physical characteristics of the environment by reducing the number of variables and rewriting the data set. The advantage of using the physically-based transformation, as described in Crist and Cicone (1984c), is that it is an invariant transformation and spectral features are consistent between scenes.

The Crist and Cicone (1984c) transformation was applied to the 1984 TM data. The results showed that almost

TABLE 5

Correlation Matrix of the Seven TM Bands for July 2, 1984

Bands	One	Two	Three	Four	Five	Six	Seven
One	1.00						
Two	0.79	1.00					
Three	0.75	0.99	1.00				
Four	0.65	0.92	0.95	1.00			
Five	0.31	0.48	0.52	0.69	1.00		
Six	-0.39	-0.17	-0.09	0.17	0.38	1.00	
Seven	-0.06	-0.17	-0.17	-0.03	0.65	0.12	1.00

every pixel the GSLD is bright, except in places where standing water was most likely present. The greenness feature was calculated using the coefficients from Crist and Cicone (1984c) and the results were consistent with the physical character of the GSLD (i.e. no greenness was found). Wetness, as derived from the Crist and Cicone (1984c) coefficients, contained the majority of the variance in the TM data, over the GSLD.

Coefficients for a physically-based transformation are relatively easy to derive. Jackson (1983) describes a method called the Gram-Schmidt process (Freidberger, 1960). The Gram-Schmidt process is the same method used by Kauth and Thomas (1976), and Crist and Cicone (1984c) for deriving coefficients. The method described by Jackson (1983) involves two distinct processes, first the coefficients are calculated from a sample of data, then the coefficients are used to rewrite the data set. The entire TM image or a selected subset of the image can be transformed with the coefficients. New coefficients were calculated in order to determine if these new coefficients, derived from the 1984 TM data of the GSLD, would contain more precise information about the physical character of the GSLD than the Crist and Cicone (1984c) coefficients. The brightness feature calculated by the process describe by Jackson (1983), were very similar to the Crist and Cicone (1984c) brightness feature. Although the new wetness

feature was generally able to separate wet from dry soil, the variation within the indicated wet and dry areas was observed to be much less than the variation produced using the Crist and Cicone (1984c) coefficients for wetness. The conclusion is that the Crist and Cicone (1984c) coefficients do produce an invariant transformation and are best for physical feature extraction from TM data. This conclusion is supported by the research and development reported in Crist and Cicone (1984a), Crist and Cicone (1984b), Crist and Cicone (1984c), and Crist et al. (1984). Also, field observations made at various times between September 1985 and October 1986, of the GSLD, support the representation of brightness and wetness one might find in the GSLD as indicated in the brightness and wetness images produced from the Crist and Cicone (1984c) coefficients.

In the development of the terrain model, the APTS data was used as the reference for both raw and image processed data. For the raw data, the APTS data was regressed against individual bands. For the processed data, the APTS data was regressed against the results of each image processing technique to determine which technique accounted for the maximum variation.

4.2 Control Point Analysis

Paramount in the model development is the positional

accuracy of TM data relative to the UTM coordinate system, as the two data sets (i.e., TM and APTS) are tied together through the UTM system. The TM data must be referenced to the UTM system through ground control points. Thus, ground control points, described is section 2.2, are the means by which TM data are combined with the APTS data. A goodness-of-fit experiment was used to test the effect of variations in the distribution of control points and the root mean square (RMS) error of the control points on the correlation between the APTS and the TM data. Due to the positional accuracy of APTS, described in section 3.1, it provided an excellent reference for the analysis of goodness-of-fit between TM data and UTM coordinates. The RMS error is a measure of how well the entire set of control points fit the UTM grid. It is the average error between the control point location and the actual UTM coordinates. A sample of the APTS profile D1-E2s consisting of 36 pixels, was used as a reference for this experiment. Four individual cases are in the test which consisted of two spatial distributions of control points. The first, referred to here as distribution 1, is illustrated in Figure 17. This distribution extends across an entire TM scene (i.e., an area covering 185 km by 185 km) and has a clustered pattern. The second, distribution 2, is represented in Figure 18. It extends over only half of a TM scene (i.e., an area covering 185 km by 92.5 km), but has more of a

```
  58. ******************************3*******************
 143. *                              1            11          1  *
 229. *                                                        1  *
 314. *                                                           1
 400. *                                           1              *
 485. *                                                          *
 571. *                                  1          1            *
 656. *                                  1    1                  *
 742. *                                   111                    *
 827. *                                    1 1 1                 *
 913. *                                    113   1     1         *
 998. *                            1                             *
1084. *                           1                              *
1169. *                           1                              *
1255. *                                                          *
1340. *                                                          *
1426. *                          1                               *
1511. *                                                          *
1597. *                            1                             *
1682. *                                                          *
1768. *                                                          *
1853. *                                  1                       *
1939. *                                  1                       *
2024. *                                  111                     *
2110. *                                                          *
2195. *                                 1     1                  *
2281. *                                   11                     *
2366. *                                  3                       *
2451. *                                                          *
2537. *                                                          *
2622. *                                                          *
2708. *                                                          *
2793. *                                                          *
2879. *                                            1 1           *
2964. *                                                          *
3050. *                                                          *
3135. *                                            1  *
3221. *                                            2  *
3306. *                                               *
3392. *                                   3      12   *
3477. *                                      1   111 *
3563. *                                  1   21  2    *
3648. *                                               *
3734. *                                               *
3819. *                                               *
3905. *                                               *
3990. *                                               *
4076. *                                               *
4161. *                                               *
4247. *                                               *
4332. *        1                                      *
4418. * 51 22                                         *
4503. 16522 1 1                                       *
4589. 139        1                                    *
4674. *442 1                                          *
4760. * 111                                           *
4845. ****11*****************************************
      11111111122222222222222333333333333334444444444445555555555555
      34566789011234556789901233456788901223456678900123455678 9
      753198642086420875319753197642086420864319753197532086420
      667890123445678901223456789011234567899012345677890123456
```

Elements (Pixel Columns)

Figure 16. Control point spatial distribution 1, 90 control points.

Lines (Pixel Rows)

```
 302. ***************************************1********************************
 335. *                                                                      *
 367. *                               1       1                              *
 400. *                                                                      *
 432. *                                                                      *
 465. *                                                                      *
 498. *                                                                      *
 530. *                                       1                1             *
 563. *              1                                                       *
 595. *                                                                      *
 628. *                    1                  1                              *
 660. *                     1                 1                      1       *
 693. *                                                            11        *
 726. *                                                                      *
 758. *                                                                      *
 791. *                    2                                1        1       *
 823. *                     11                1            1                 *
 856. *              1      21                1                      1       *
 889. *                                                            11 *
 921. *                     11                1                              *
 954. *                                                                      1
 986. *                          1                                          *
1019. *                                                            1 1
1052. *                          1                                 2*
1084. *                                                            *
1117. *                                                            *
1149. *                                                            *
1182. *       1                                                    *
1214. *                                                            *
1247. *                                                          1 *
1280. *       1                       1                            1
1312. *1       1       1              1                            1
1345. *                                                            *
1377. *                                                            *
1410. *                               1                            *
1443. *                                                            *
1475. *       1                                                    *
1508. *          1                                                 *
1540. *                                                            *
1573. *     2        11  1                                         *
1606. *     1           1                  1                       *
1638. *      1                                                     *
1671. *      1           1                                         *
1703. *    1   1                                                   *
1736. * 11  1                                                      *
1769. * 11                                                         *
1801. 1 111                                                        *
1834. *    1                                                       *
1866. * 11                                                         *
1899. *  21                                                        *
1931. *      1                                                     *
1964. *   21                                                       *
1997. *     1                                                      *
2029. *     1                                                      *
2062. * 11    1                                                    *
2094. *      1                                                     *
2127. **1*********************************************************************
      1111112222222222233333333333334444444444445555555555566666
      567899012345667890123345678900123456778901234456789011234
      542109765421097654210976542109765421087653210876532108765
      529742974196419631863185530853075207529742974196419631 8631
```
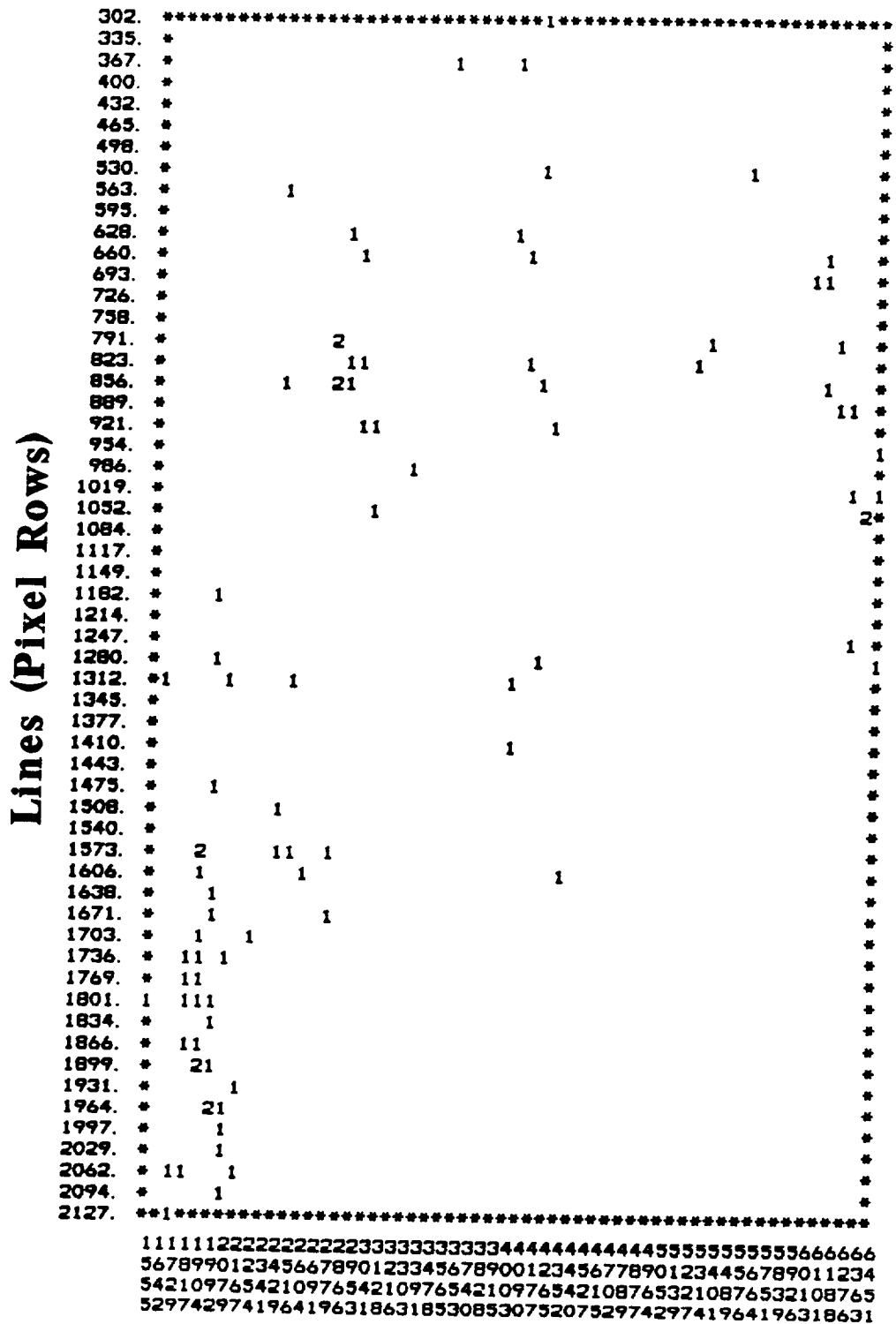
Elements (Pixel Columns)

Figure 17. Control point spatial distribution 2, 122 control points.

uniform pattern to the distribution of control points.

The first goodness-of-fit test employed distribution 1 and 122 control points with an RMS error of 23 meters. The correlation coefficient between the APTS and the TM data in this test was 0.86. The second goodness-of-fit test also used distribution 1, with only 68 control points and an RMS error of 15 meters, the correlation coefficient was improved to 0.91. The third test used distribution 2 and 90 control points with an RMS error of 15 meters, resulting in a further improvement in the correlation coefficient to 0.93. The fourth test also used distribution 2 and 60 control points with an RMS error of 11 meters, but the correlation coefficient remained at 0.93. Based on the results of this experiment, the 90 control points from distribution 2, with an RMS error of 15 meters and a correlation coefficient of 0.93, were used in all subsequent analysis. The justification for selecting this set of control points is as follows: this set of control points share the highest correlation coefficient with the set of control points that has the lowest RMS error. Also, the goodness-of-fit test 2, using distribution 1, when compared to the goodness-of-fit test 3, using distribution 2, shows that the RMS error is not an absolute measure of goodness-of-fit. As the above analysis indicates, having 30 more control points with a more uniform distribution produces a more reliable fit between the TM data and the

UTM system.

Another analysis of the control points was done using a program within ELAS, called CSPA. This program computes statistics concerning the influence of the spatial distribution of control points on the accuracy of the image to map registration (Graham, 1980). CSPA uses the nearest neighbor technique to examine the statistical distribution of control points (i.e., random, uniform, or clustered). Table 6 shows the results of the CSPA analysis of the four tests of goodness-of-fit. It is apparent from the standard variate of the normal curve parameter (C) (see Table 6) that the control points selected have the most uniform distribution. The standard error of the mean distribution (Sigma E) increases as the number of control points is reduced, and the mean distance to the nearest neighbor expectation (R(E)) increases, indicating the possibility of large areas that are void of control points. The CSPA analysis supports the above selection of the control points for use in further analysis.

4.3 Comparative Analysis of the Two TM Images

Analysis of the two TM images, July 2, 1984 and June 19, 1985, was carried out to determine which image was better able to provide the most accurate quantitative

TABLE 6

Results of the Control Point Spacing Analysis (CSPA)

	Distribution 1		Distribution 2	
	RMS 23m	RMS 15m	RMS 15m	RMS 11m
n	122	64	90	60
R(A)	59.26	106.0	91.34	85.04
R(E)	210.8	271.8	158.0	189.6
R	0.281	0.390	0.578	0.449
Sigma E	9.98	17.23	8.71	12.79
C	15.19	9.62	7.66	8.17

n - Number of control points.
R(A) - Mean distance to the nearest neighbor.
R(E) - Mean distance to the nearest neighbor expectation.
R - Degree departure from random expectation.
Sigma E - Standard error of the mean distribution.
C - Standard variate of the normal curve parameter.

information about the morphometry of the terrain. All seven bands of the pixels that coincide with the APTS profiles B5-B4, C2-D1, C5-A5, D3-D1, E3-C1, and D1-E2s were used in this analysis. The correlation coefficients resulting from the regression of the APTS pixel elevations to the digital values of the seven bands for those pixels, from the two images, are presented in Table 7. Table 7 shows that band 7 is the TM band that is most consistent over the highly variable terrain included in this analysis. Although band 5 shows some promise, its potential usefulness is diminished by the fact that band 5 and band 7 are highly auto-correlated and therefore band 5 contains only a minimum of new information not already represented by band 7. The correlation coefficients in Table 7 also show that the July 2, 1984 data are more likely to provide accurate quantitative information about the morphometry of the terrain than the June 19, 1985 data.

The field conditions appear to be the reason for the relationship between the July 2, 1984 data and the morphometry of the terrain. On June 19, 1985 it appears that there was less soil moisture present in the GSLD then on July 2, 1984. Although, field data was not collected during the overpass of the satellite on June 19, 1985, the known physical characteristics of the reflected light energy in the mid-infrared bands (i.e.,bands 5 and 7) would indicate that with less soil moisture the light energy

TABLE 7

Correlation Coefficients for the APTS Profile Elevations and
the Seven Bands of the Two TM Images

Band	B5-B4		C2-D1		C5-A5	
	1984	1985	1984	1985	1984	1985
One	-0.35	-0.32	0.22	-0.25	0.32	-0.55
Two	-0.34	-0.82	0.36	-0.64	0.42	-0.58
Three	-0.32	-0.80	0.40	-0.66	0.47	-0.50
Four	-0.12	-0.74	0.46	-0.53	0.61	-0.34
Five	0.45	0.54	0.60	-0.21	0.71	-0.06
Six	0.40	0.59	0.09	0.78	0.14	0.83
Seven	0.75	-0.02	0.71	-0.32	0.70	-0.29
n	238		148		208	

Band	D3-D1		E3-C1		D1-E2s	
	1984	1985	1984	1985	1984	1985
One	-0.24	0.00	0.29	0.24	0.63	0.09
Two	-0.73	-0.12	-0.10	0.14	0.63	0.23
Three	-0.71	0.09	-0.04	0.25	0.70	0.37
Four	-0.68	-0.08	0.00	0.24	0.82	0.59
Five	0.80	0.81	0.79	0.62	0.90	0.70
Six	0.66	-0.22	0.23	0.05	0.40	0.70
Seven	0.87	0.83	0.87	0.61	0.93	0.63
n	638		694		36	

n = number of pixels in the profile.

would be much more uniformly reflected from all topographic feature in the GSLD (e.g., between the basin floor and higher topographic features such as dunes). To illustrate the character of the reflected light from the topographic features in the GSLD, a surface plot of band 7, in 1984, is displayed in Figure 18. This plot is representative of the reflect light energy from the salt flats and dunes located near Knolls, Utah, located a few miles north of Interstate 80. APTS profile B5-B4 runs through the approximate center of this plot, (Figure 18). Figure 19 is a plot of band 7, in 1985, over the same area as that shown in Figure 18. The shape of the reflectance surface in 1984, (Figure 18), is much closer to the actual topography than that of the 1985 data, (Figure 19), as determined by the APTS profile and the U.S. Geological Survey 1:24000-scale Orthophoto Map.

Contour lines from the 1:24,000-scale Orthophoto Map published by the U.S. Geological Survey, were digitized and compared to the TM data. The contour interval of the orthophoto map is 5 feet (1.5 meters). Although some error has been introduced during the digitizing process and the griding process (i.e. the digitized data must be converted into grid cell format before plotting), Figure 20 does represent the topography as described by the 1:24,000 scale contour map. When comparing TM band 7 1984, (Figure 18), to the digitized orthophoto map, (Figure 20), one can see the potential for significant amounts of additional information
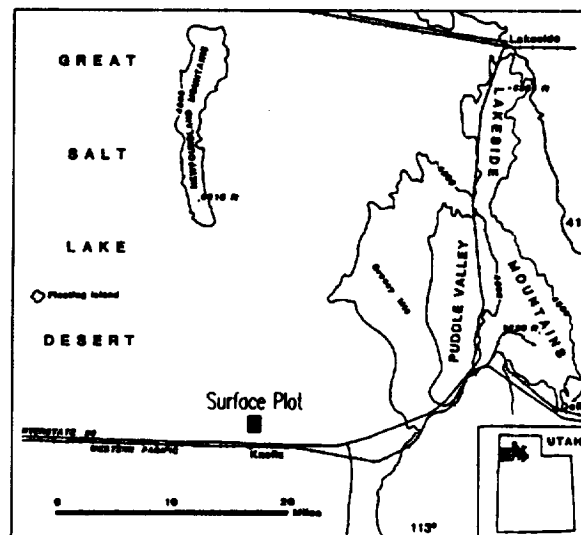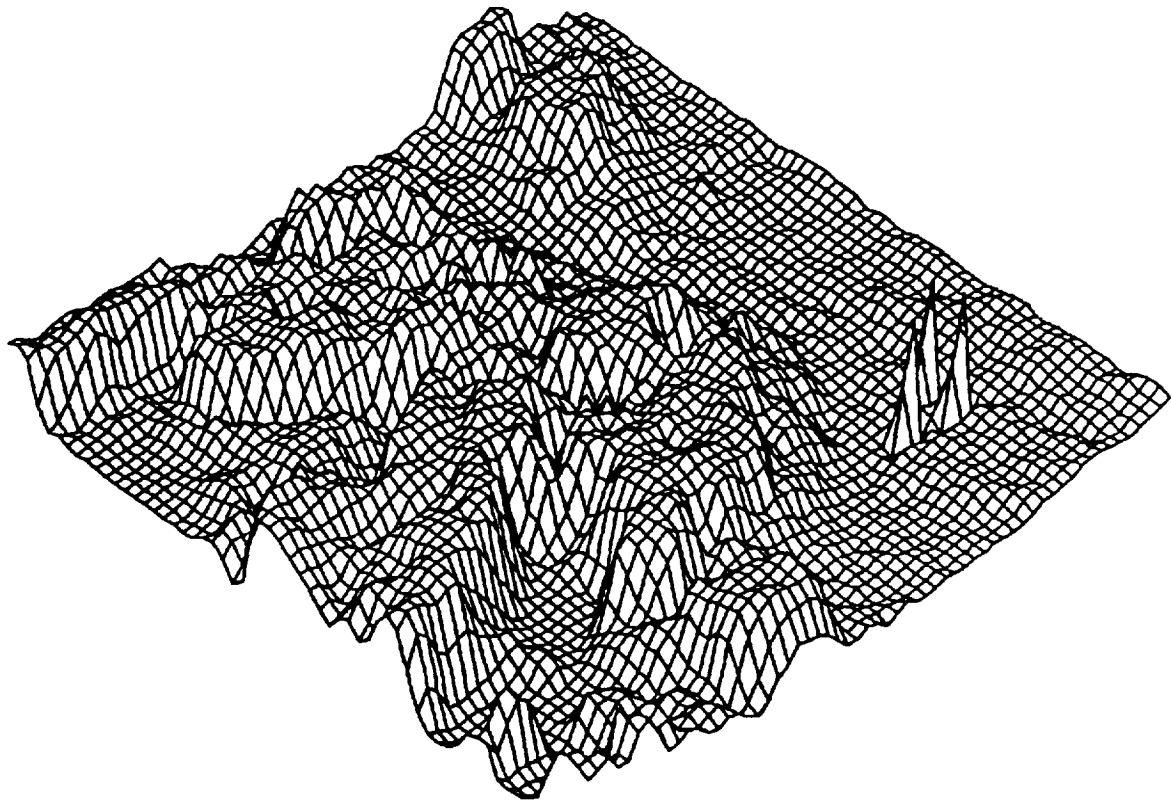
Figure 18. Surface plot of band 7 1984, from the dunes and salt
flats located near Knolls, Utah. APTS profile B5-B4
runs through the approximate center of this plot,
from right to left.
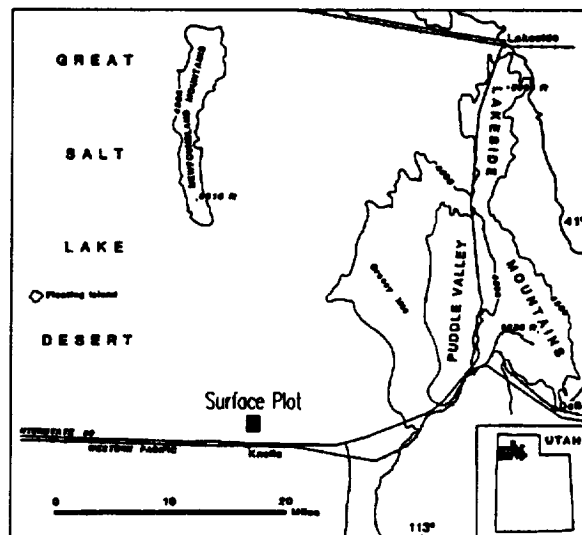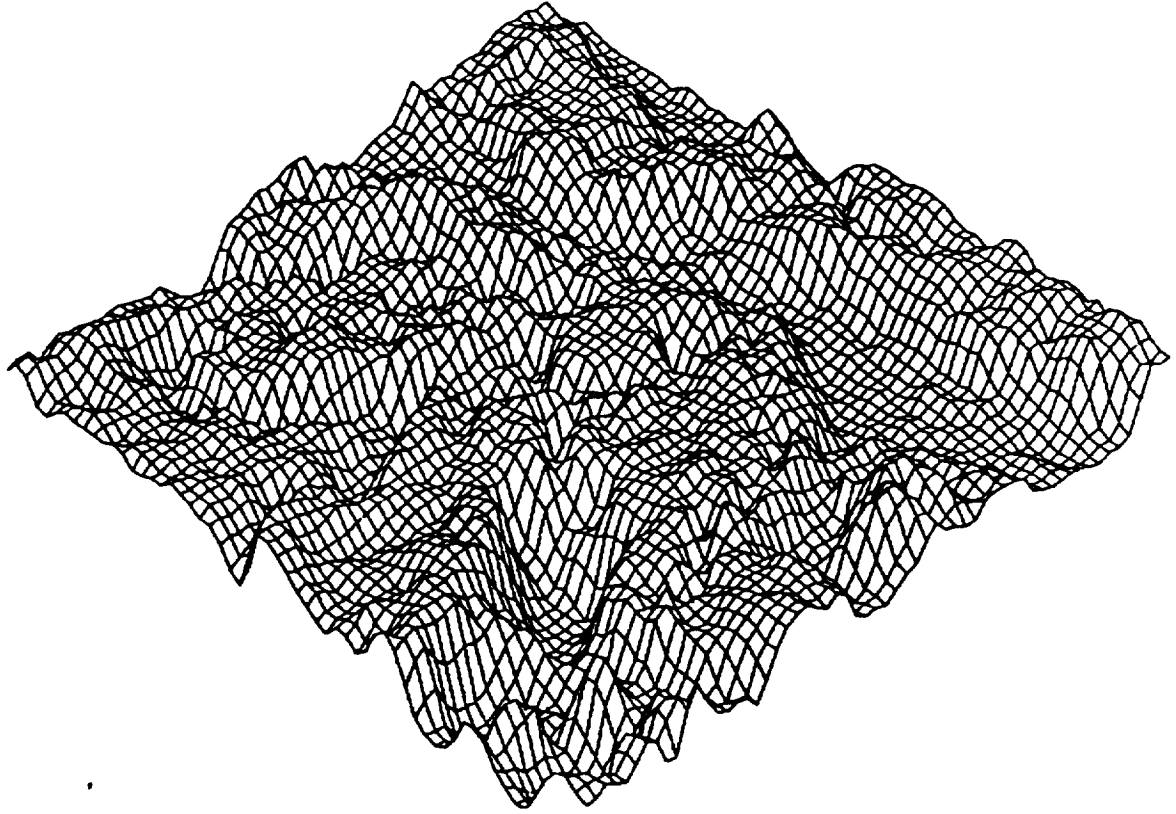
Figure 19. Surface plot of band 7 1985, from the dunes and salt flats located near Knolls, Utah. APTS profile B5-B4 runs through the approximate center of this plot, from right to left.
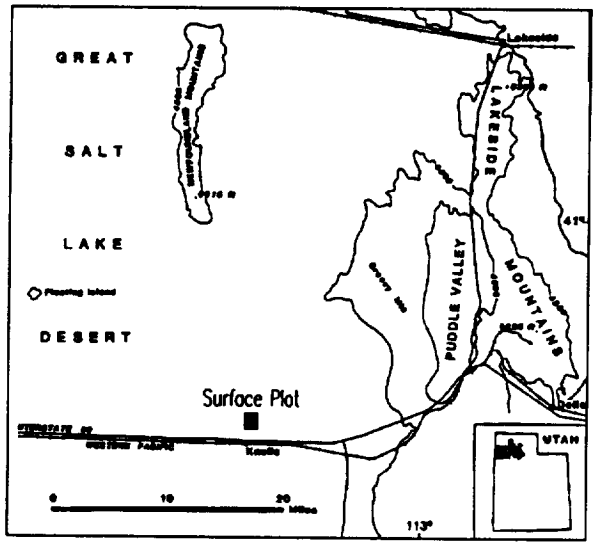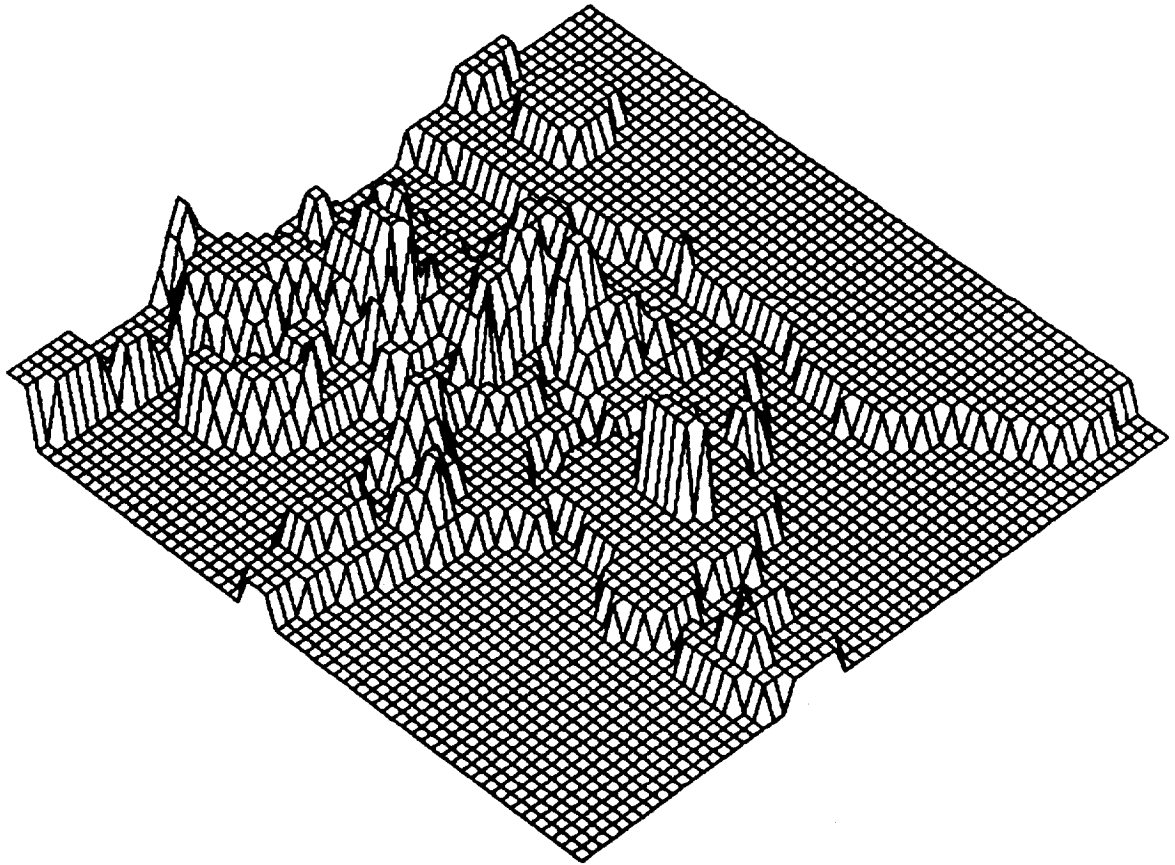
Figure 20. Surface plot of digitized topography from the USGS
map in the Knolls, Utah area. APTS profile B5-B4
runs, from right to left, through the approximate
center of this plot.

about the terrain that could be extracted from TM band 7, 1984.

The above analysis shows that band 7 of the July 2, 1984 TM image has the most consistent relationship with terrain morphometry. Although, bands 2, 3, and 4 of the June 19, 1985 TM image have high correlations to APTS profile B5-B4, (Table 7), band 7, July 2, 1984, also has a high correlation to this profile. Since band 7, July 2, 1984, provides the most consistent relationship to terrain morphometry and thus allows for the development of a terrain model that would be most widely applicable to the features of interest in the GSLD, all subsequent terrain modeling efforts included the use of the July 2, 1984 TM data, to the exclusion of the June 19, 1985 TM data.

Three spikes appear on the right of Figure 19, it is not known what caused this phenomena. Since the characteristics of the TM sensor have been well studied, as stated in section 2.1, and no sensor related noise has been found that is similar to this phenomena -- most likely its not sensor related noise, but is caused by something on the ground. If it were sensor related noise one would expect the values of these spikes to reach the maximum value of 255, they do not. However, the reason for there existence is not of importance to this study, but it is interesting to track the changes in the spikes as the plots of various processing techniques are presented.

CHAPTER 5

CONCLUSION

5.1 Image-Based Terrain Model

The development of the image-based terrain model consisted of applying the results of the data structure analysis to a model of the terrain. The image-based terrain model is developed from an understanding of the information content. With an understanding the information content and image processing techniques, physical and image features are extracted from the TM data and then incorporated into the unmodified band 7 data so it will represent more accurately the morphometry of the terrain.

The image-based terrain model relies heavily on band 7. This is due to the amount of information band 7 contains about the terrain morphometry. However, there are some weaknesses in the rendering of the terrain by band 7. The upper surfaces of the geomorphic features, between 1288m (4225 ft) and 1289m (4230 ft) above mean sea level, are an area of weakness in the band 7 image-based terrain model. Characteristics of the upper surfaces of the geomorphic features such as, standing vegetation density, vegetative litter, surface roughness, or soil color, may be

influencing the detection of the terrain morphometry by band 7.

Analysis of the 5/7 band ratio, after the DVs have been inverted, showed that it depicted the upper surfaces of the geomorphic features better than band 7 alone. Figure 21 is a surface plot of the 5/7 ratio, for the same area as Figure 18. When Figure 21 is compared to Figure 18, one can see that the upper surfaces in Figure 21 are much less irregular than in Figure 18. It appears that the affects of the upper surface characteristics of the geomorphic features have been reduced by the 5/7 band ratio allowing the morphometry of the terrain to be detected.

During analysis it was observed that band 6 is able to separate the basin-floor from the geomorphic features very distinctly and consistently. This is most likely a result of the apparent temperature gradient between the basin-floor and the geomorphic features, and the resampling, from the 120m by 120m pixel to the 30m by 30m pixel which allows for a distinctive boundary between features at the pixel resolution of the other TM bands. It was found that band 6 could be used as a guide for the modification of band 7 where upper surfaces of geomorphic features occurred, band 7 would be replaced by the 5/7 band ratio as determined by band 6. After careful visual analysis of band 6 it was found that the DV of 186 defined the boundary between the basin-floor and the geomorphic features. DVs equal to and
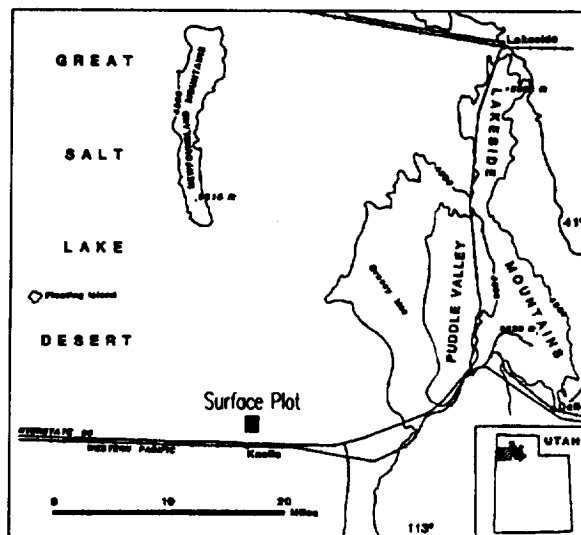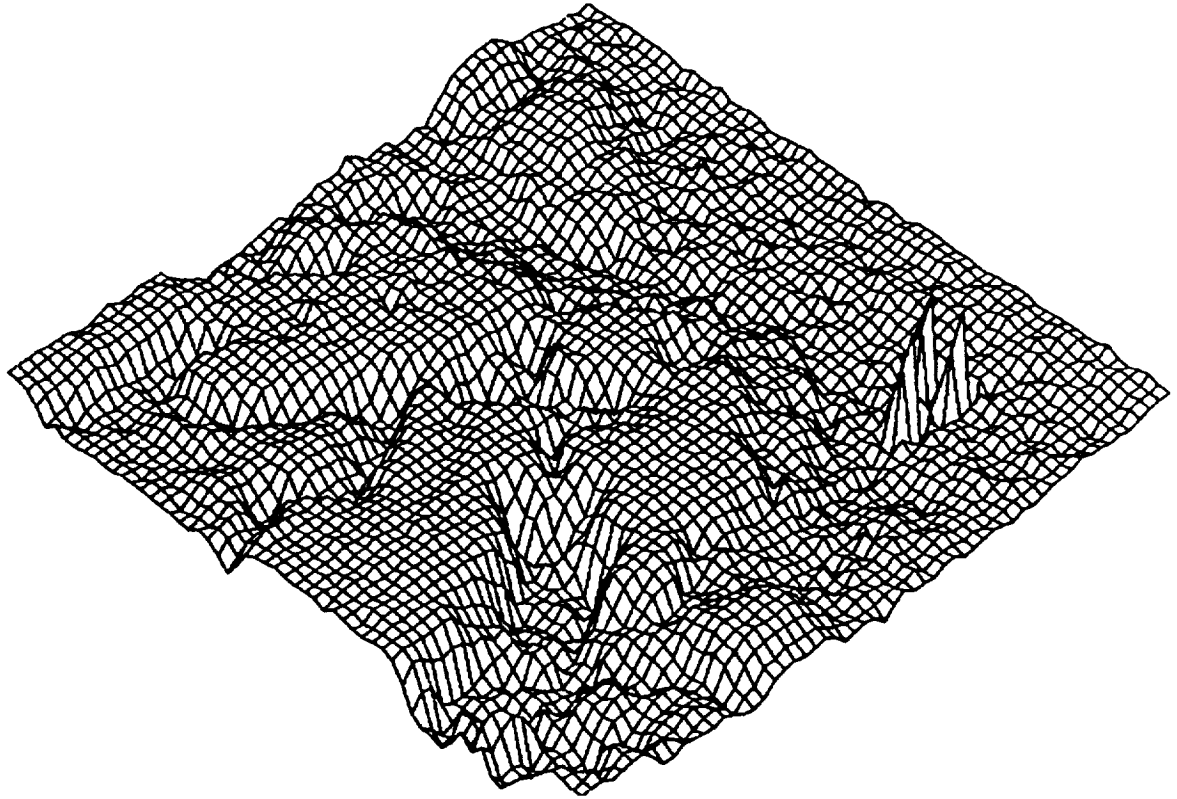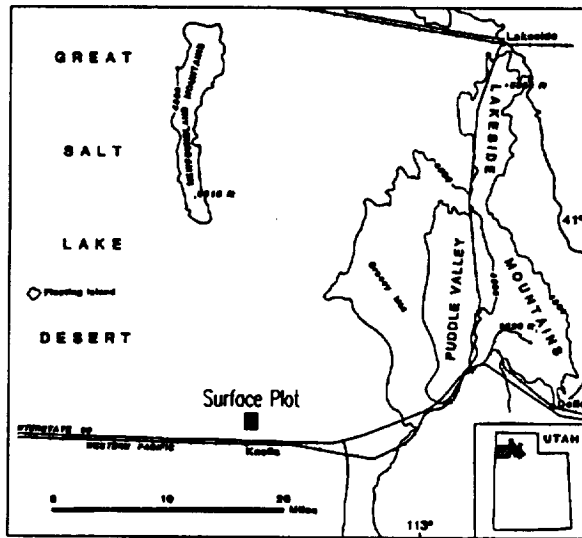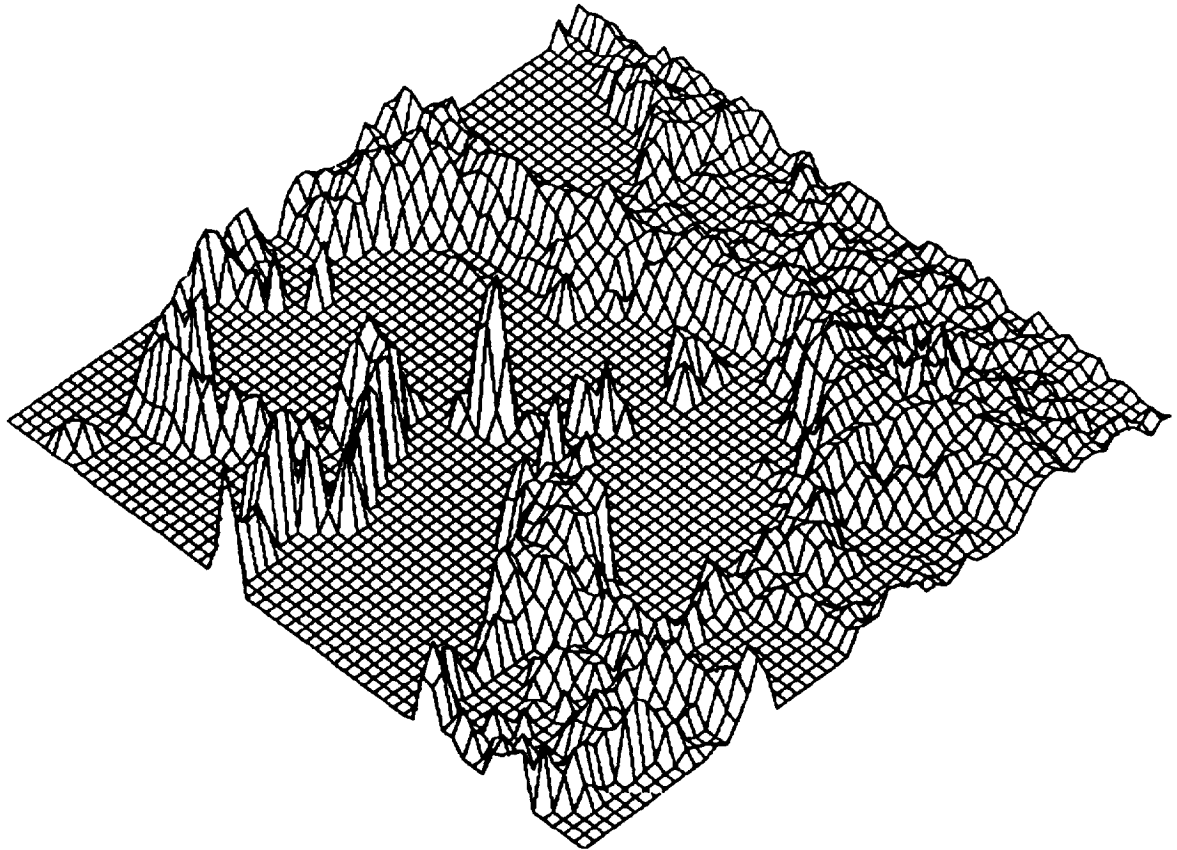
Figure 21. Surface plot of the 5/7 ratio from the dunes and salt
flats located near Knolls, Utah. APTS profile B5-B4
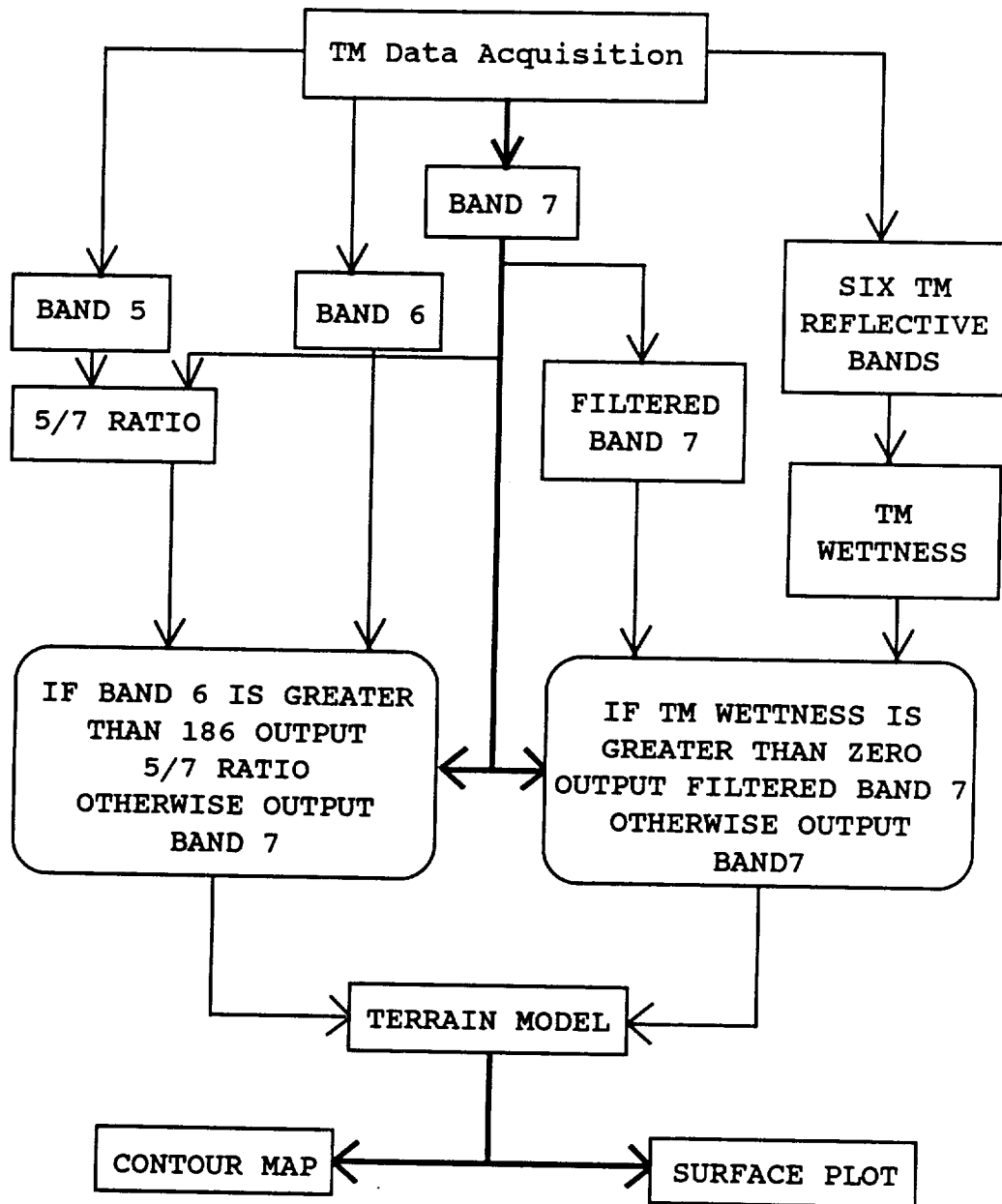runs, from right to left, through the approximate
center of this plot.

above 186 identify the upper surfaces of sand dunes and other features, while DVs below 186 identify the basin-floor.

Another source of weakness in the band 7 image-based terrain model occurs at the trimline, where the basin-floor meets the costal geomorphic features in the GSLD. It appears as though there is a consistent pattern of moisture accumulation at the trimline. The affect of this phenomenon on band 7 is in the form of an anomalous absorption of light energy resulting in the appearance of a dip or trench-like feature around sand dunes, where none exists. In figures 14 and 15, arrows are used to denote the affects of the increased absorption in band 7. Also, Figure 18 shows the results of this phenomenon, one can see a trench-like feature on the left side of the plot. This phenomenon was detected very well by the TM wetness feature, derived from the Crist and Cicone (1984c) coefficients. Figure 22 is a surface plot of TM wetness, the higher the value the greater the 'wetness'. It was found that by applying a lowpass image filter to band 7 the majority of the affects of this anomalous absorption could be removed.

With the above analysis complete the following image-based terrain model was developed. This model involves steps that are independent of one another as well as steps that must be in sequence. Figure 23 diagrams the steps involved in the image-based terrain model. To begin a

Figure 22. Surface plot of TM wetness, from the dunes and salt
flats located near Knolls, Utah. APTS profile B5-B4
runs, from right to left, through the approximate
center of this plot.

```
                    ┌─────────────────────┐
                    │ TM Data Acquisition │
                    └─────────────────────┘
                              │
                              ▼
                         ┌─────────┐
                         │ BAND 7  │
                         └─────────┘

    ┌─────────┐      ┌─────────┐                          ┌──────────────┐
    │ BAND 5  │      │ BAND 6  │                          │   SIX TM     │
    └─────────┘      └─────────┘                          │  REFLECTIVE  │
         │                │                               │    BANDS     │
         ▼                │      ┌──────────────┐         └──────────────┘
    ┌─────────┐           │      │  FILTERED    │                │
    │ 5/7 RATIO│          │      │  BAND 7      │                ▼
    └─────────┘           │      └──────────────┘         ┌──────────────┐
                          │             │                 │     TM       │
                          │             │                 │  WETTNESS    │
                          │             │                 └──────────────┘
         │                │             │                        │
         ▼                ▼             ▼                        ▼
  ╭────────────────────────╮     ╭──────────────────────────╮
  │  IF BAND 6 IS GREATER   │     │  IF TM WETTNESS IS       │
  │  THAN 186 OUTPUT        │◄──►│  GREATER THAN ZERO       │
  │  5/7 RATIO              │     │  OUTPUT FILTERED BAND 7  │
  │  OTHERWISE OUTPUT       │     │  OTHERWISE OUTPUT        │
  │  BAND 7                 │     │  BAND7                   │
  ╰────────────────────────╯     ╰──────────────────────────╯
           │                              │
           └──────────┐        ┌──────────┘
                      ▼        ▼
                 ┌───────────────────┐
                 │  TERRAIN MODEL    │
                 └───────────────────┘
                      │        │
      ┌───────────────┘        └───────────────┐
      ▼                                         ▼
┌──────────────┐                        ┌──────────────┐
│ CONTOUR MAP  │                        │ SURFACE PLOT │
└──────────────┘                        └──────────────┘
```

Figure 23. Flow diagram of the steps invoved in the image-based
terrain model.

lowpass digital image filter is applied to band 7 to smoothing the image slightly. Then, the pixels in the original, unfiltered band 7 data are replaced with the filtered data only where wetness is present -- as determined from the TM wetness feature calculated from the Crist and Cicone (1984c) coefficients. Results of the above filtering and modifications, to band 7, were tested against APTS profile B4-B5; the correlation coefficient improved from .75 to .77. Next, the 5/7 ratio was calculated and inverted, so as to produce a positive relation with the topography, then a lowpass filter was applied to the 5/7 ratio and the final step is a replacement of pixels in the original band 7 data with the filtered 5/7 ratio data where band 6 DVs are greater than 186.

The combined results of all the steps in the model were tested against the APTS data and the correlation coefficient was improved to .81. This modeling technique constructs layers of image features from the TM data and then laminates the layers together in appropriate ways that enhance the information content of the original data. Figure 24 is a plot of the above model. The Image-based terrain model was verified against two APTS profiles not used in the model development. One APTS profile used for verification was B5-C4, this profile has 283 pixel elevations. The correlation coefficient of band 7 to APTS
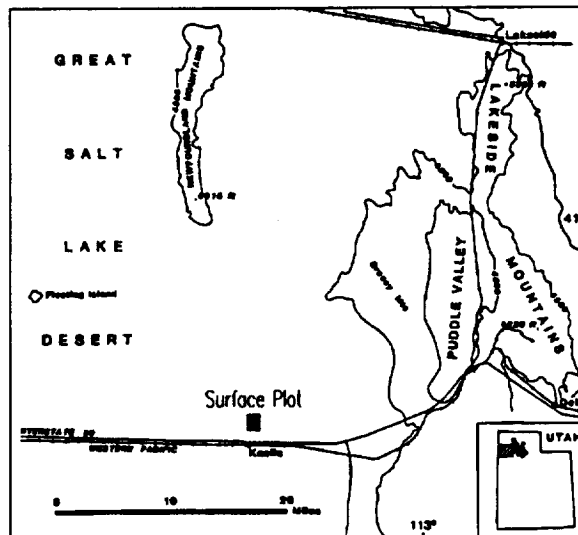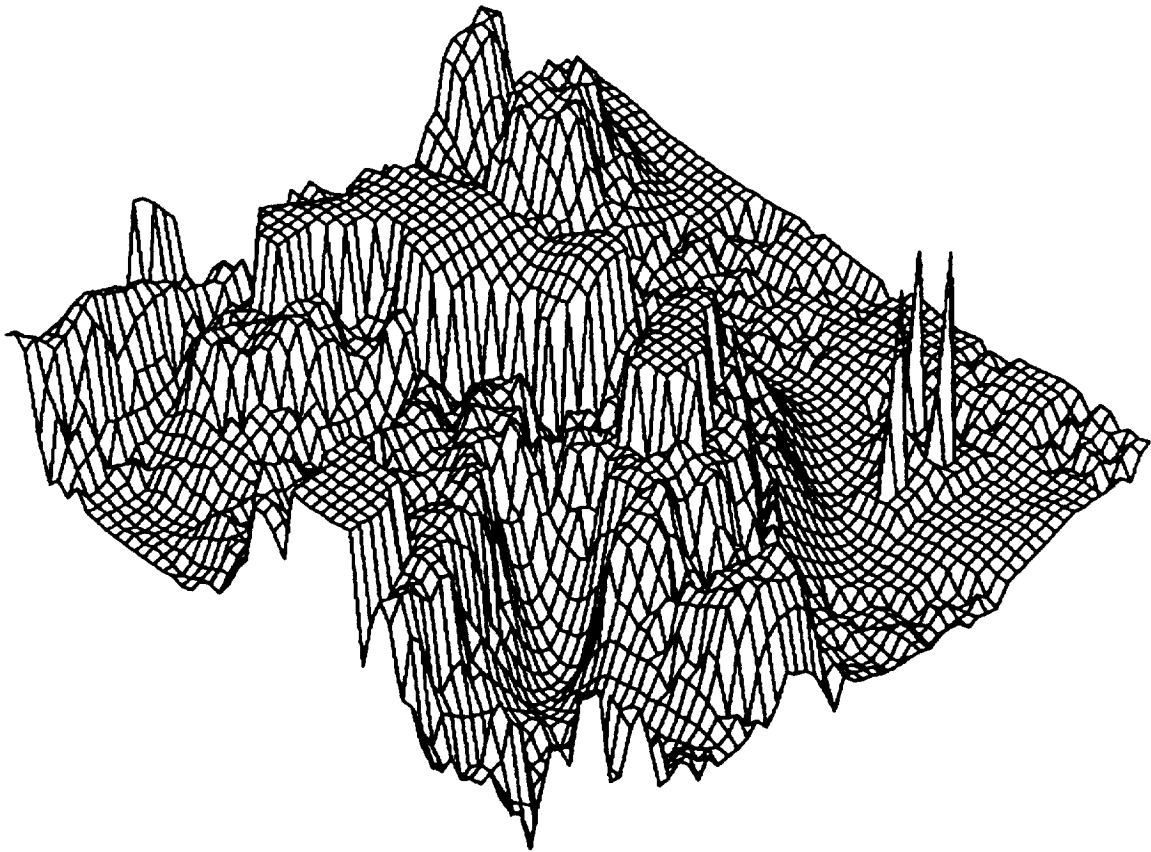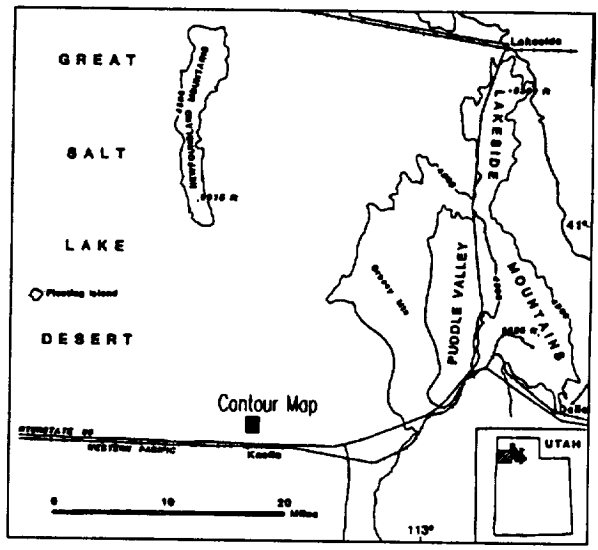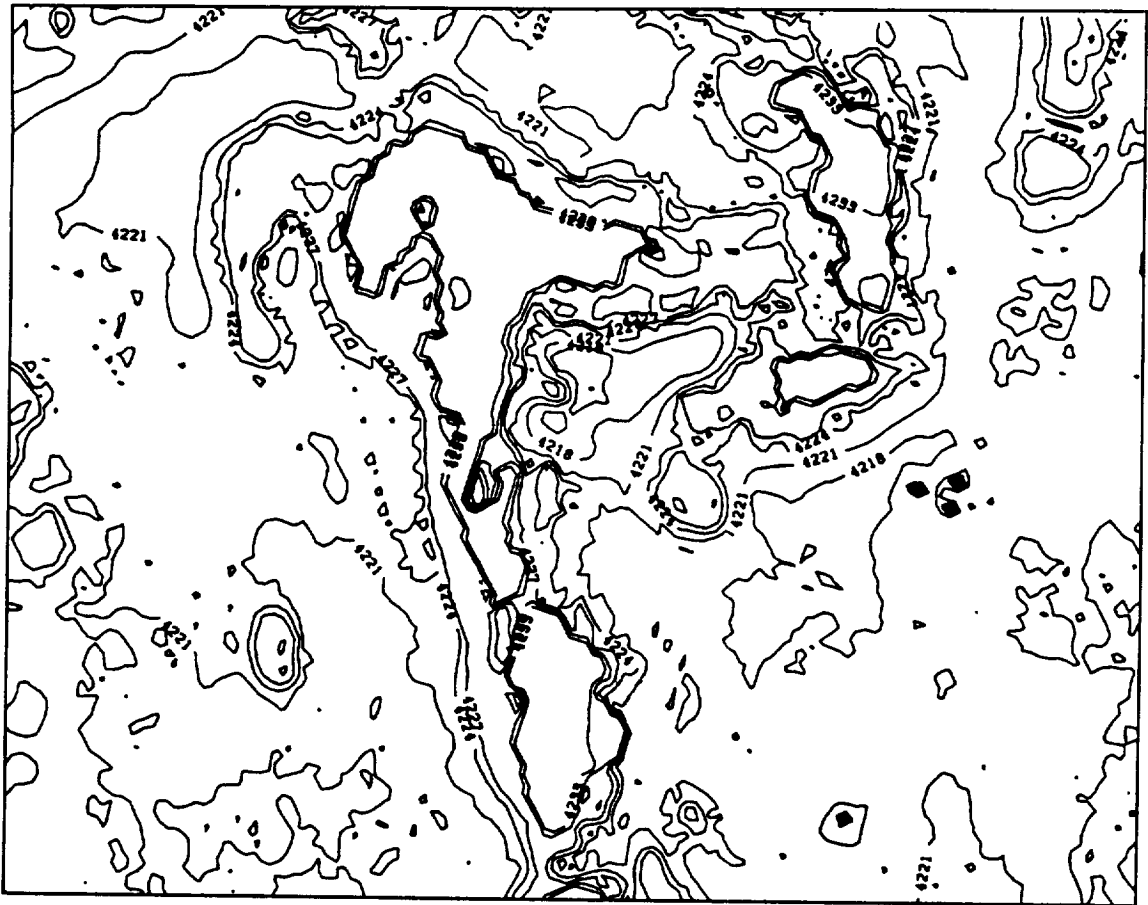
Figure 24. Surface plot of the image-based terrain model results for the Knolls, Utah, area. APTS profile B5-B4 runs, from right to left, through the approximate center of this plot.

Profile B5-C4 is 0.73 and the correlation coefficient of the terrain model to APTS profile B5-C4 is 0.79. Another APTS profile used for verification was C4-C5, this profile has 302 pixel elevations. The correlation coefficient of band 7 to APTS profile C4-C5 is 0.46 and the correlation coefficient of the terrain model to APTS profile C4-C5 is 0.47.

These results indicate that the degree of increased information gained by using the terrain model over just band 7 appears to by dependent on the initial correlation to band 7.

5.2 Terrain Mapping

The three-dimensional surface plots are very valuable for interpreting the geomorphology of the terrain. The terrain represented by these plots can be rotated and tilted, and viewed from many perspectives. These plots are limited by the hardware and only a very small portion of data can be displayed at one time. Although, much larger plots at the same scale can be produced on bigger plotters, the amount of data represented is controlled by what can be displayed in perspective without obscuring features that are of interest. The plots are also limited by the fact that there is no absolute spatial reference; therefore, these plots are not maps. However, a unique method was

developed, as part of this research, to produce contour maps of large areas from TM data at any scale.

In order to produce contour maps that can be plotted at any scale, the TM data must be referenced to the UTM projection. The mapping coefficients described in section 2.2 are used to convert the TM image coordinates to UTM geographic coordinates for mapping. The contouring technique developed during this research avoids the resampling and rotation of the pixels necessary to convert gridded data (e.g., TM image data) from one coordinate system to another. As each pixel is analyzed for contouring the TM image coordinates for that pixel are converted into UTM coordinates, thereby eliminating a significant amount of error introduced to gridded data during resampling and rotation. The resampling and rotation is analogous to trying to force the bricks in a wall to side by one another slightly and change size.

The regression equation derived from the APTS data can also be applied to the DV of each pixel as it is processed for contouring. The result is a geographically referenced contour map of topography, representing the morphometry of the terrain. Figure 25 is a contour map of approximately the same area as in Figures 18, 19, 20, 21, 22, and 24. The regression equation has been applied to the terrain model results to produce contours every 3 feet. Geomorphic features can be readily identified, such as sand dunes.

Figure 25. Contour plot of the image-based terrain model results
for the Knolls, Utah area. APTS profile B5-B4 runs,
from right to left, through the approximate center
of this plot. The Contour interval is every 3 feet
and the contour map is scale 1:24,000.

This map was produced at a scale of 1:24,000. At this time only five 7.5 minute, 1:24,000 scale map, have been mapped; however, all the 7.5 minute map for the GSLD could be produced as needed.

5.3 Summary

The goal of this research has been to model selected costal geomorphic features by extracting information from remote sensing measurements. This goal has been approached from two directions. One direction involves technical development, and the other involves information extraction from remote sensing measurements and modeling of terrain.

Technical developments include the incorporation of APTS data in satellite image analysis, and the production and use of three-dimensional surface plots of TM reflectance data. Also included in the technical developments is the analysis of the ground control point spatial distribution and its affects on geometric correction, and the terrain mapping procedure, using satellite data, that eliminates the need to degrade the data by resampling.

The information extraction from remote sensing measurements included a methodological approach to analysis of the multi-dimensional data structure of TM; identification of the data structure containing the

information of interest and the extraction of this information for the image-based terrain model. Finally, the image-based terrain model provides quantitative information about the terrain morphometry based on the physical relationship between TM data, the physical character of the GSLD, and the APTS measurements.

The GSLD is an excellent 'laboratory' for research involving remote sensing data. Future researchers may want to include with there data collection the use of spectral radiometers. Spectral radiometers give one the ability to study the light reflectance characteristics of earth's surface materials under various controlled experiments, in the field and in the laboratory. This would enable researchers to better understand the physical relationship between the surface materials and light reflectance. Also, research of the hydrologic character of the GSLD, and the influence of soil moisture variations on TM, needs to be investigated in more detail. Researchers should include the collection of soil samples and field spectrometer data, at the time of the satellite overpass, in such investigations.

APPENDIX

SCATTER DIAGRAMS OF THE SIX REFLECTIVE

THEMATIC MAPPER BANDS

Plot of Band1 vs Band2
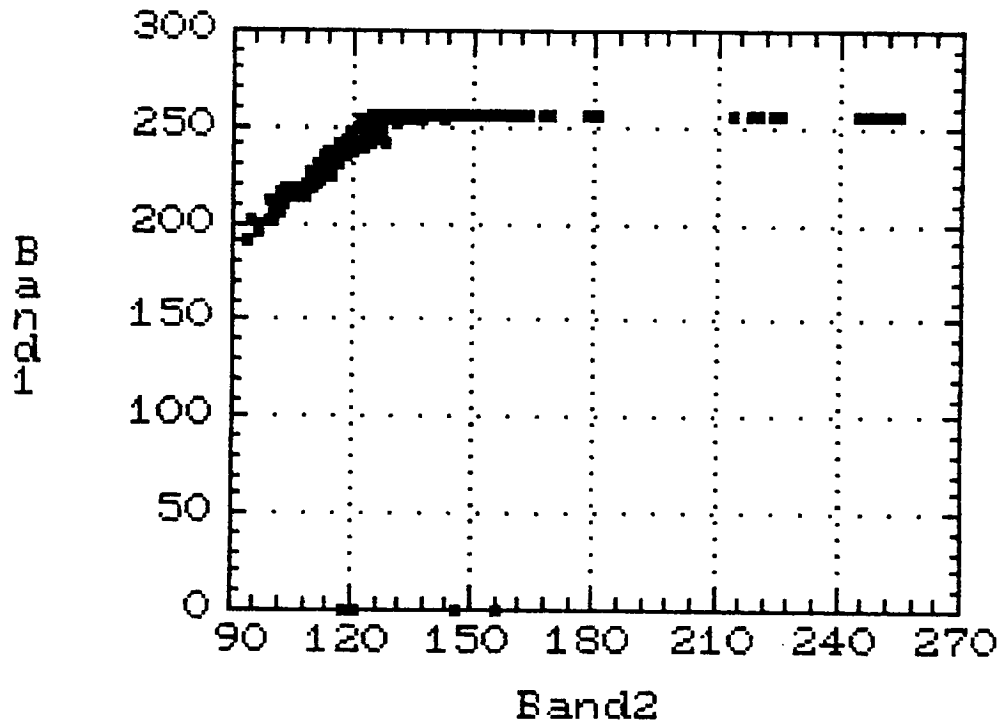
Plot of Band1 vs Band3
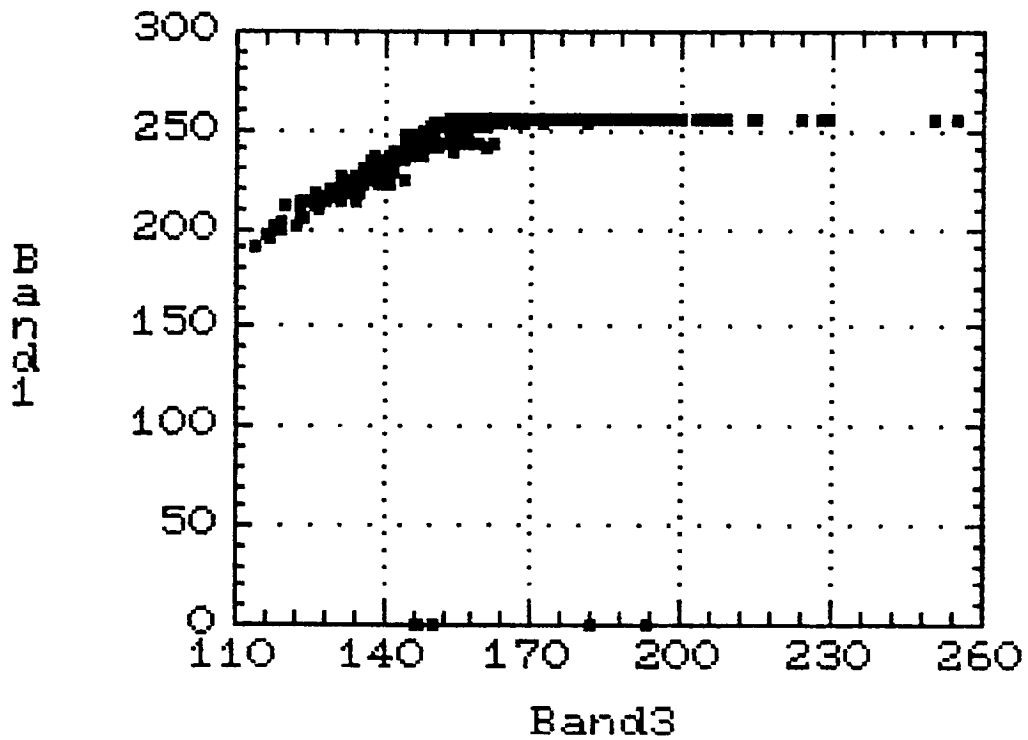
Plot of Band1 vs Band4
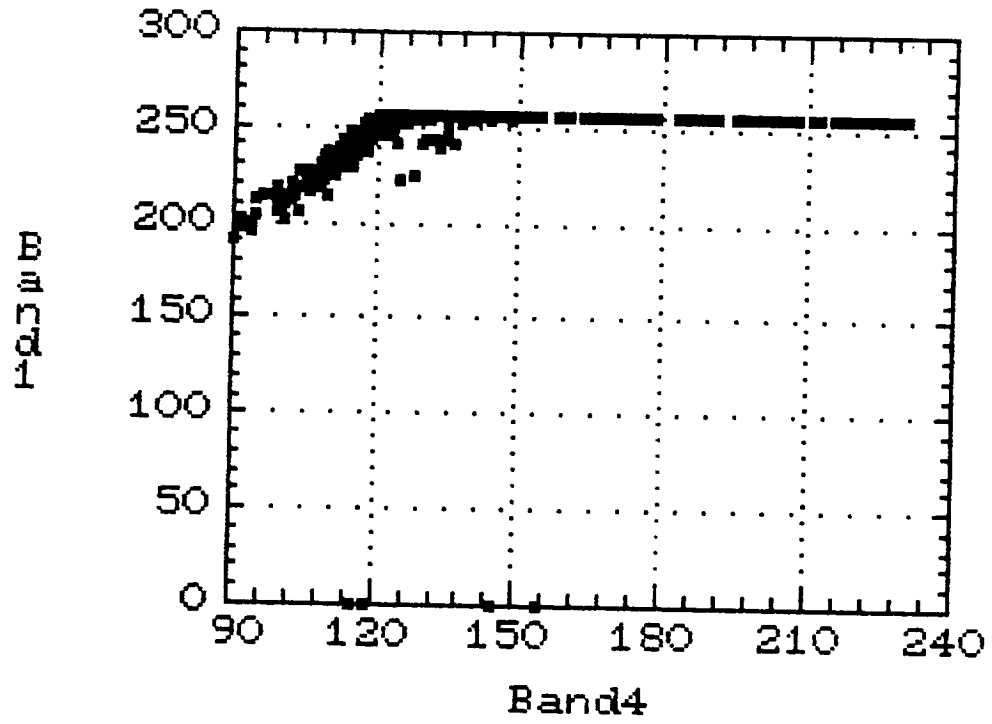
Band4

Plot of Band1 vs Band5
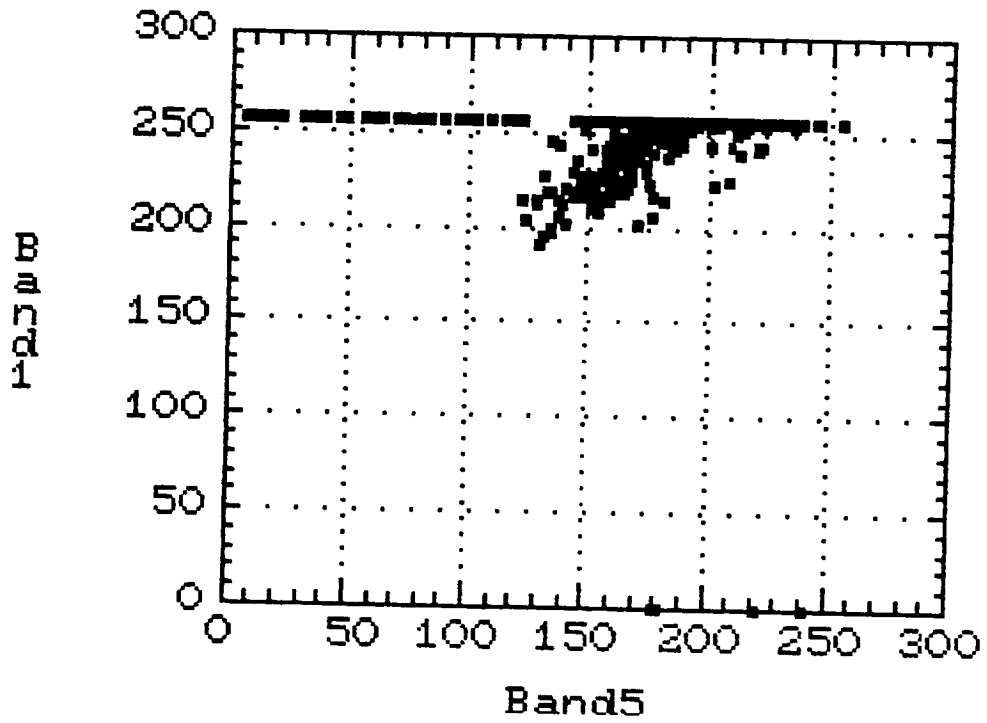
Band5

Plot of Band1 vs Band7
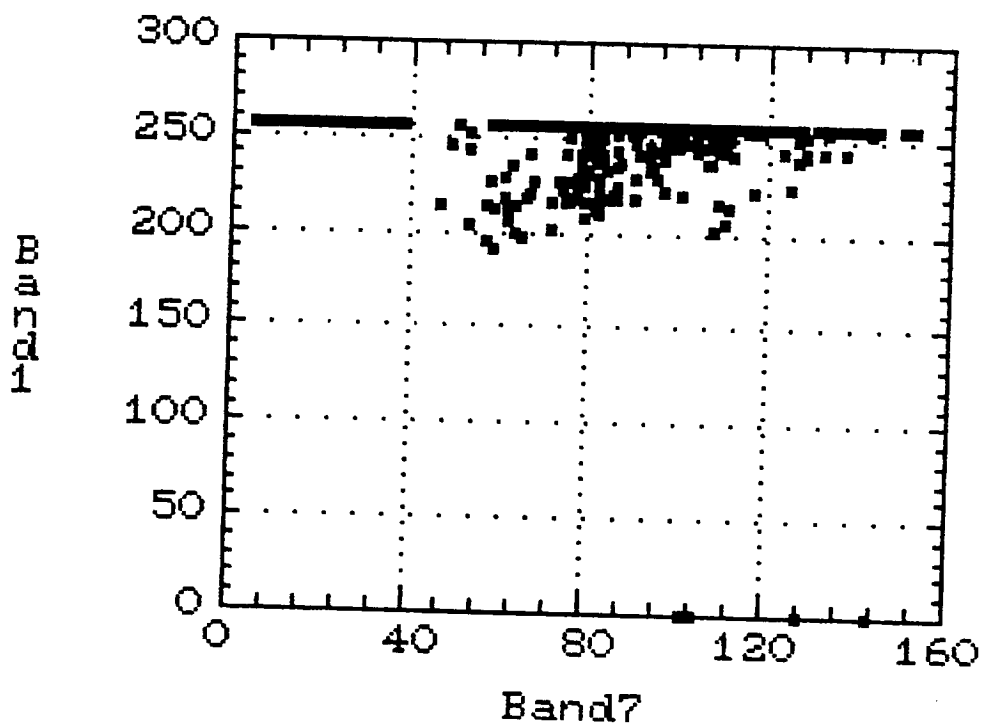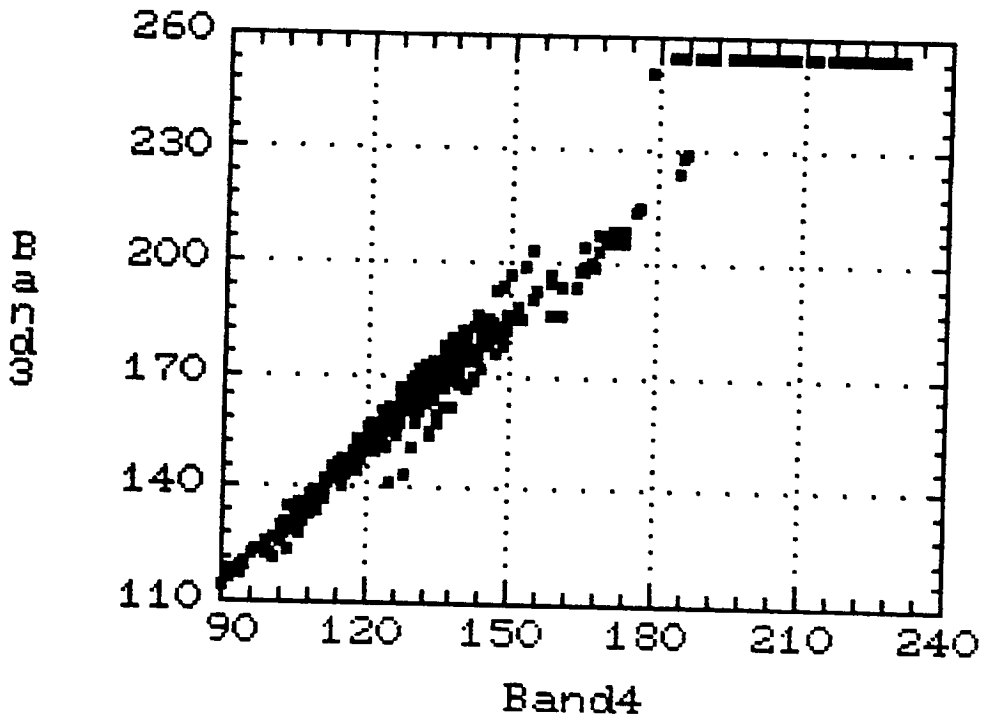

Plot of Band2 vs Band3
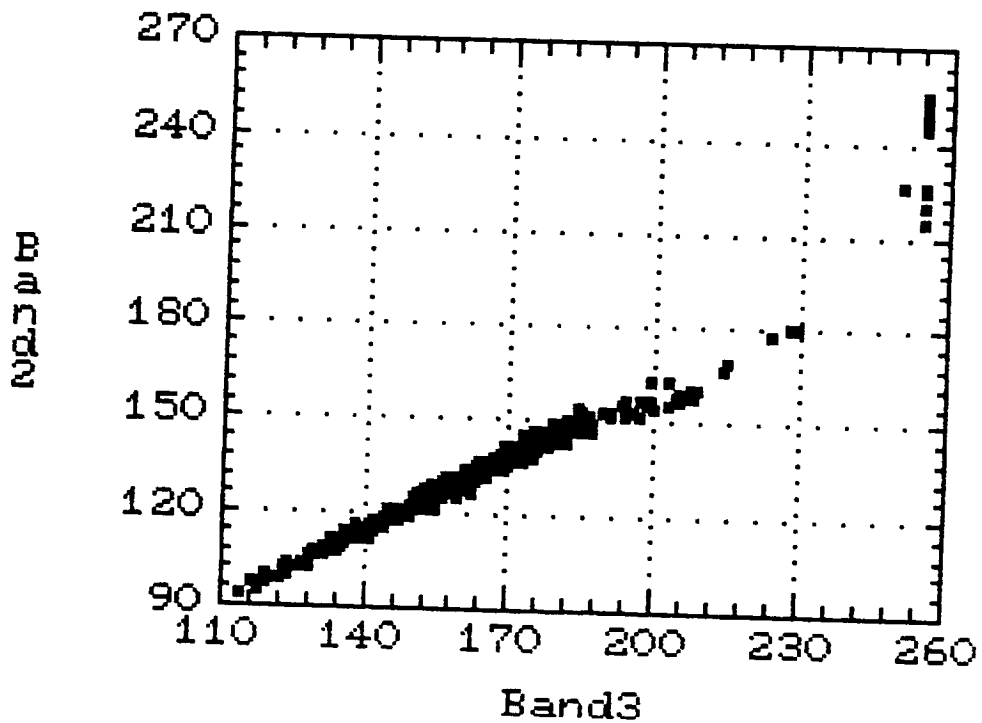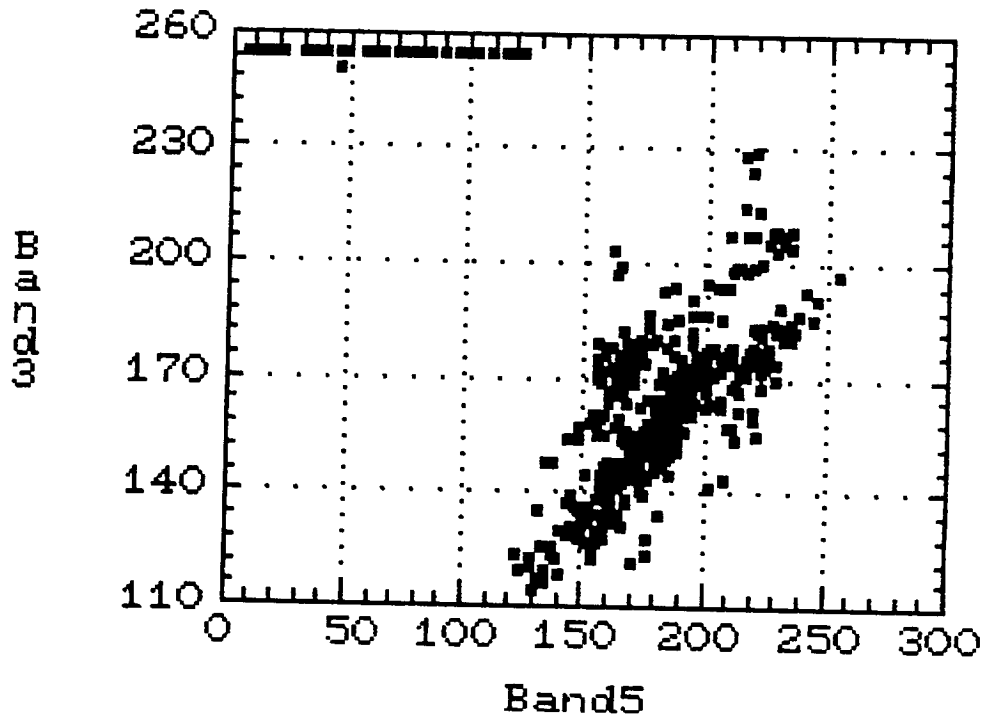
Plot of Band2 vs Band4
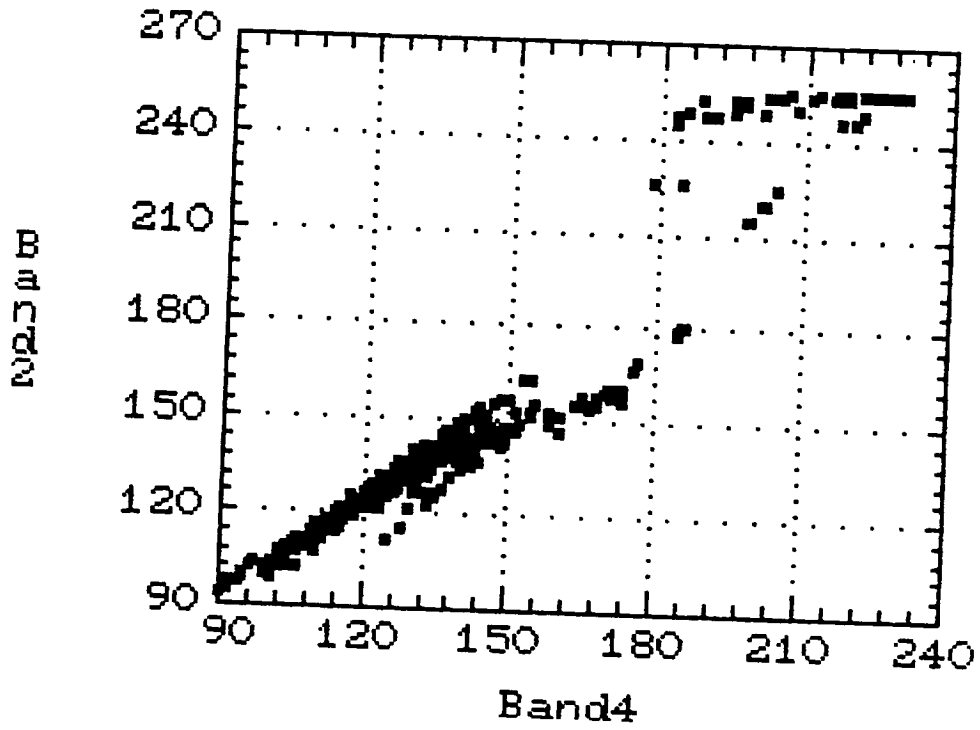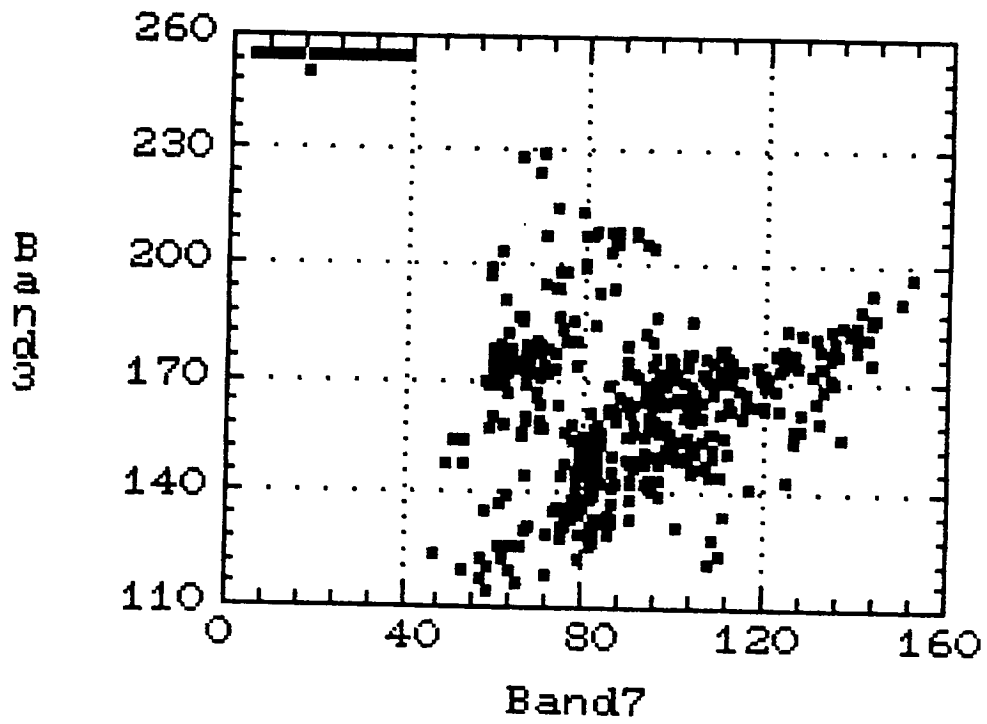

Plot of Band2 vs Band5
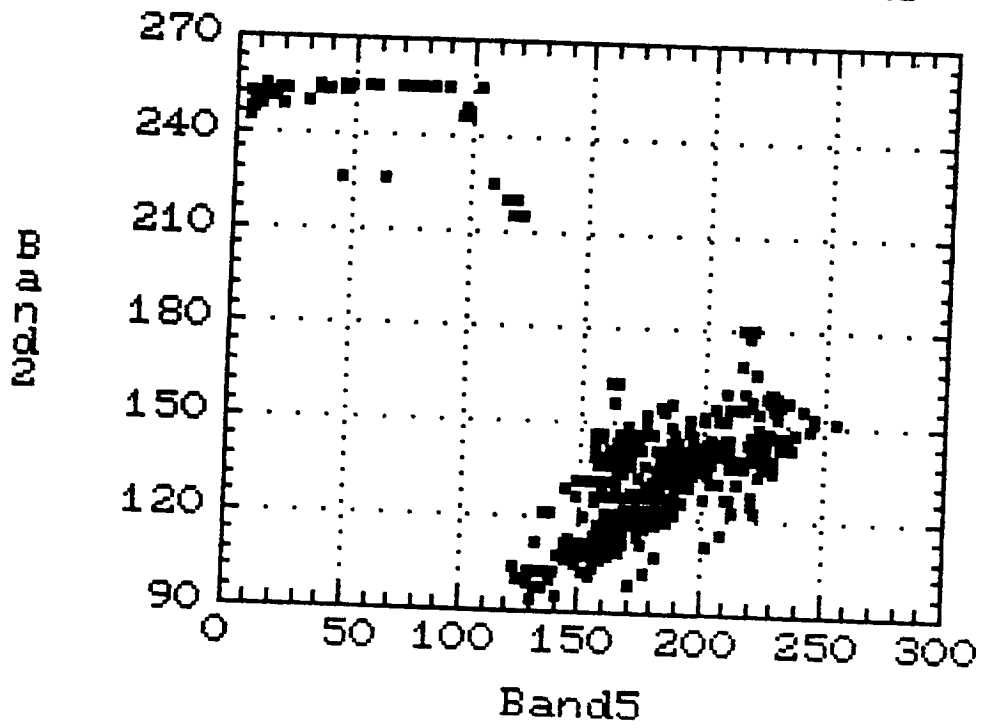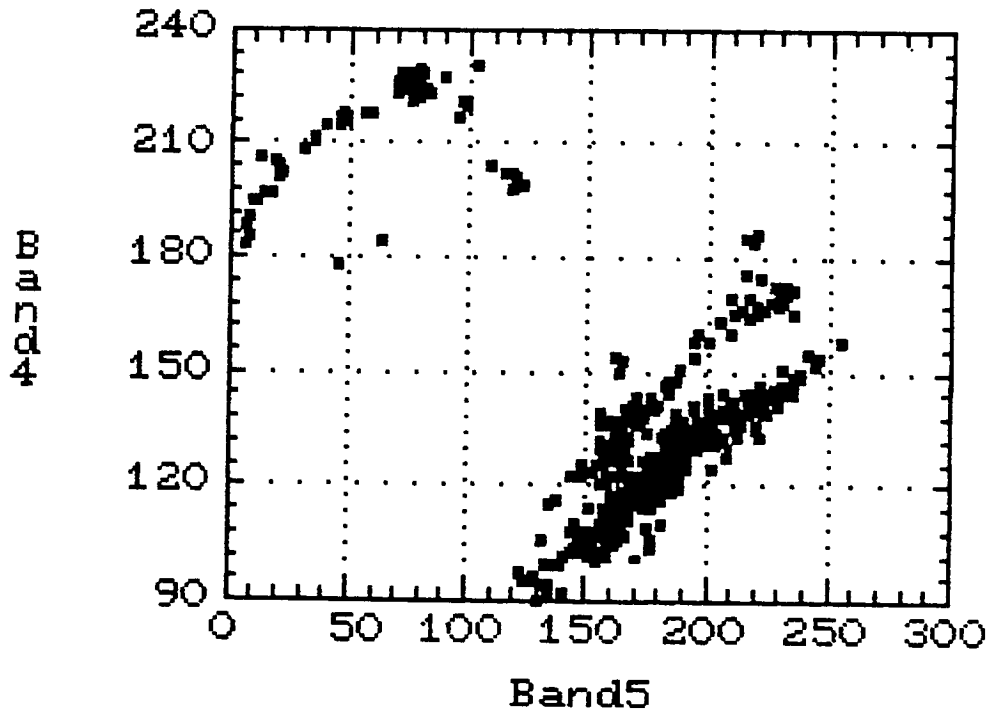
Plot of Band2 vs Band7
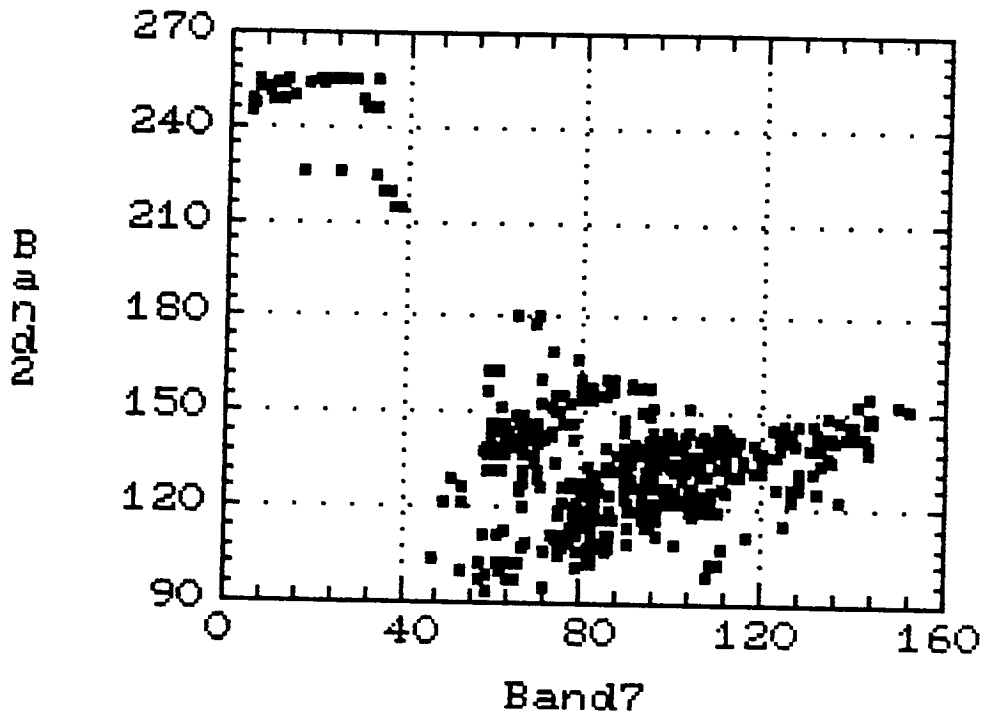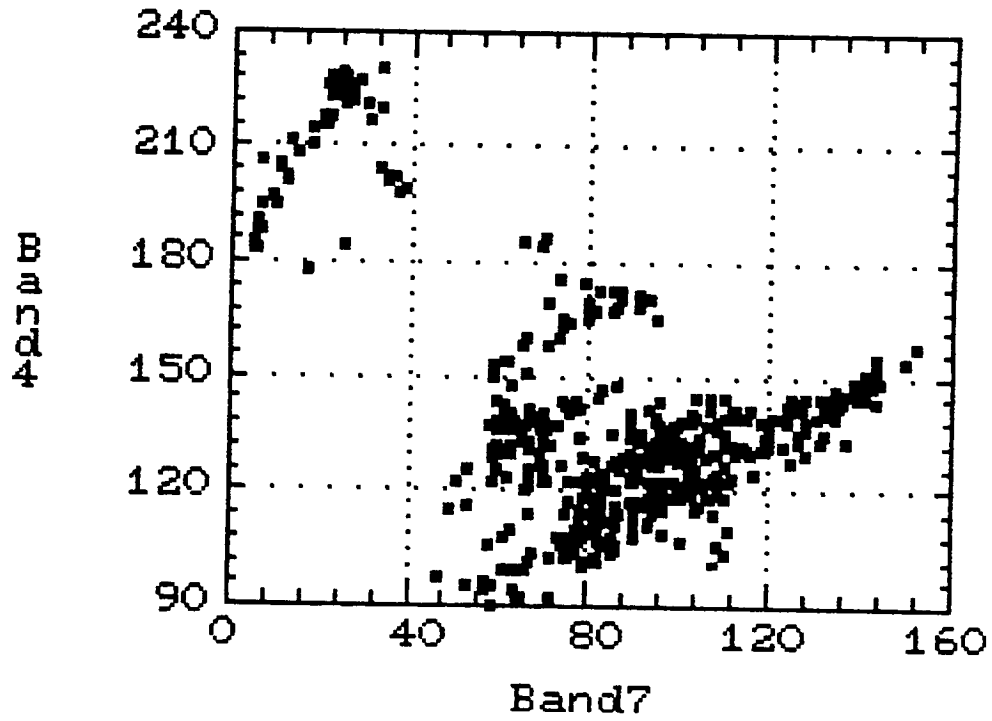

Plot of Band3 vs Band4
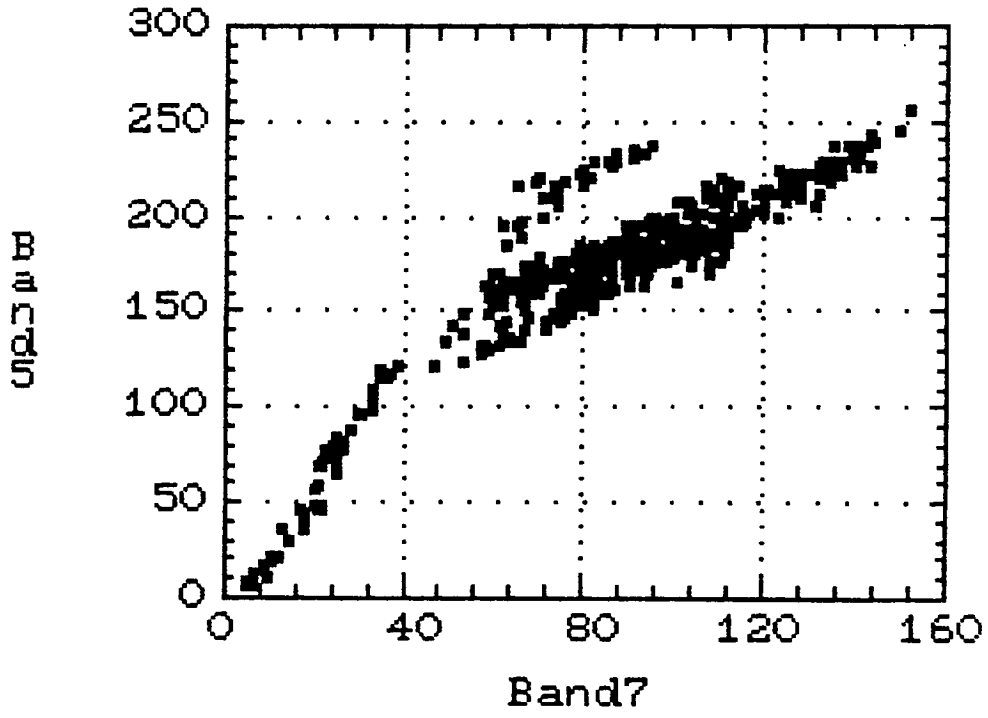
Plot of Band3 vs Band5

Plot of Band3 vs Band7

Plot of Band4 vs Band5

Plot of Band4 vs Band7

Plot of Band5 vs Band7

REFERENCES

Becker F., P. Ramanartsizehence and M. Stoll. 1985. "Angular Variation of the Bidirectional Reflectance of Bare Soils in the Thermal Infrared Band," Applied Optics, Vol. 2 no. 3, pp. 365-375.

Bunnik, N.J.J. 1978. "The Multi-Spectral Reflectance of Shortwave Radiation by Agricultural Crops in Relation with Their Morphological and Optical Properties," H. Veeman Zoan B. B., Wageningen, Netherlands.

Campbel, J.B., R.M. Haralick, and S. Wang. 1984. "Interpretation of topographic Relief from Digital Multispectral Imagery," Proceedings of the Society of Photo-Opical Instrumentation Engineers. Vol. 475, pp. 98-116.

Colwell, J.E. 1981. "Landsat Feature Enhancemant: Or, can we Seperate Vegetation from Soil?," Proceedings of the 15th International Symposium of Remote Sensing of the Environment, ERIM, Ann Arbor, Michigan, pp. 599-621.

Chapman, W.H. 1986. "Profiling the Great Salt Lake Desert with the Aerial Terrain Profiling of Terrain System (APTS)," U.S. Geological Survey Open-File Report, 17 p.

Cooper, K.D. and J.A. Smith. 1985. "A Monte Carlo Reflectance Model for Soil Surfaces with Three-Dimensional Structure," IEEE Transactions on Geoscience and Remote Sensing, Vol. GE-23, pp. 668-673.

Crist, E.P, and R.C. Cicone. 1984a. "Application of The Tasseled Cap Concept to Simulated Thematic Mapper Data," Photogrammetric Engineering and Remote Sensing, Vol. 50, pp. 343-352.

Crist, E.P, and R.C. Cicone. 1984b. "Comparisons of the Dimensionality and Features of Simulated Landsat-4 MSS and TM Data," Remote Sensing of Environment.

Crist, E.P., and R.C. Cicone. 1984c. "A Physically-Based Transformation of Thematic Mapper Data - The TM Tasseled Cap," IEEE Transactions on Geoscience and Remote Sensing, Vol. GE-22, pp. 256-263.

Crist, E.P., R. Laurin, J.E. Colwell, and R.J. Kauth. 1984. "Investigations of Vegetation and Soils Information Contained in Landsat Thematic Mapper and Multispectral Scanner Data," Final Report, Environmental Research Institute of Michigan, Ann Arbor, Michigan. NASA contract No. NAS9-16538.

Cyran, E.J. 1983. "Aerial Profiling of Terrain System," Journal of Surveying Engineering, Vol. 109, No. 2, pp. 136-150.

Davis, J.C. 1973. "Statistical and Data Analysis in Geology," New York: John Wiley & Sons, Inc.

Donna, J.I. 1985. "Aerial Profiling of Terrain System Applications Test Report Great Salt Lake Desert Profiling Project Results," Charles Stark Draper Laboratory Report, CSDL-R-1813, Cambridge, MA, 60 p.

Eaton, F.D. and I. Dirmhirn. 1979. "Reflected Irradiance Indicators of Natural Surfaces and Their Effect on Albedo," Applied Optics, Vol. 18, pp. 994-1008.

Eliason, P.T., T.J. Donovan, and P.T Chavez. 1981. "Extraction of Topographic and Spectral Albedo Information from Multispectral Images," Photogrammetric Engineering and Remote Sensing, Vol. 47(1), pp. 1571-1579.

Elvidge, C.D. and R.J.P. Lyon. 1985. "Influence of Rock-Soil Spectral Variation on the Assessment of Green Biomass," Remote Sensing of Environment, Vol. 17, pp. 265-279.

Fraser R.S. and Y.J. Kaufman. 1985. "The Relative Importance of Aerosol Scattering and Absorption in Remote Sensing," IEEE Transactions on Geoscience and Remote Sensing, Vol. GE-23, no. 5, pp. 625-633.

Freiberger, W.F., Ed. 1960. "The International Dictionary of Applied Mathematics," Van Nostrand, Princeton, NJ, p. 412.

Graham, M.H., G. Junkin, M.T. Kalcic, R.W. Pearson, and B.R. Seyfarth. 1980. "ELAS: Earth Resources Laboratory Applications Software," Two Volumes, January 1986 revision, ERL Report 183, National Aeronautics and Space Administration, National Space Technology Laboratories, Earth Resources Laboratory, NSTL, Mississippi.

Haralick, R.M., and K. Shanmuga. 1973. "Computer Classification of Reservior Sandstones," IEEE Transactios on Geoscience and Remote Sensing, Vol. GE-11, pp. 171-173.

Haralick, R.M. 1973. "Glossary and Index to Remote Sensing Image Pattern Recognition Concepts," Pattern Recognition. Vol. 5, pp. 391-403.

Huete, A.R., R.D. Jackson and D.F. Post. 1985. Spectral Response of a Plant Canopy With Different Soil Backgrounds. Remote Sensing of Environment. Vol. 17, pp. 37-53.

Jackson, R.D. 1983. "Spectral Indices in N-Space," Remote Sensing of Environment. Vol. 13, no. 5, pp. 409-421.

Kauth, R.J., and G.S. Thomas. 1976. "The Tasseled Cap - A Graphic Description of Spectral-Temporal Development of Agricultural Crops as Seen by Landsat," Proceedings of the Symposium on Machine Processing of Remotely Sensed Data, LARS, Purdue University, West Lafayette, Indiana, pp. 41-51.

Kimes D.S. 1983. "Dynamics of Directional Reflectance Factor Distributions for Vegetation Canopies," Applied Optics, Vol. 22, no.9, pp. 1364-1372.

Kimes D.S., W.W. Newcomb, J.B. Schutt, P.J. Pinter, Jr. and R.D. Jackson. 1984. "Directional Reflectance Factors Distributions of a Cotton Row Crop," International Journal of Remote Sensing, Vol. 5, no. 2, pp. 263-277.

Kimes, D.S., J.M. Norman and C.L. Walthall. 1985. "Modeling Radiant Transfers of Sparse Vegetation Canopies," IEEE Transactions on Geoscience and Remote Sensing, Vol. GE-23, no. 5, pp. 695-704.

Li, X.W., and A.H. Strahler. 1985. Geometric-Optical Modeling of a Conifer Forest Canopy," IEEE Transactions on Geoscience and Remote Sensing, Vol. GE-23, no. 5, pp. 705-721.

Malila, W.A. and M.D. Metzler. 1984. "Themetic Mapper Radiomateric Characterization," Proceedings of The Tenth International Symposium on Machine Processing of Remotely Sensed Data, June 12-14, 1984.

Mamon G., D.G. Youmans, Z.G. Sztankay, and C.E. Mongan. 1978. "Pulsed GaAs Laser Terrain Profiler," Applied Optics, Vol. 17, no. 6, pp. 868-877.

Norman, J.M., J.M. Welles and E.A. Walter. 1985. "Contrasts Among Bidirectional Reflectance of Leaves, Canopies, and Soils," IEEE Transactions on Geoscience and Remote Sensing, Vol. GE-23, no. 5, pp. 659-667.

Perry, C.R., and L. F. Lautenschlager. 1984. "Functional Equivalence of Spectral Vegetation Indices," Remote Sensing of Environment, Vol. 14, pp. 169-182.

Podwysocki, M.H., D.B. Segel, and M.J. Abrams. 1983. "Use of Multispectral Scanner Images for Assessment of Hydrothermal Alteration in the Marysvale, Utah, Mining Area," Ecomonic Geology, Vol. 78, pp. 675-678.

Proceedings of the Science Characterization Early Results Symposium. 1983. NASA Goddard Space Flight Center, Greenbelt, MD, Feb. 1983.

Prost, G. 1980. "Alteration Mapping with Airborne Multispectral Scanners," Economic Geology, Vol. 75, pp. 894-906.

Ranson K.J., C.S.T. Daughty, L.L. Biehl and M.E. Bauer. 1985. Sun-View Angle Effects on Reflectance Factors of Corn Canopies Remote Sensing of Environment, Vol. 18, pp. 147-161.

Reyna, E. and Badhewar, G.D. 1985. Inclusion of Specular Reflectance in Vegetative Canopy Models. IEEE Transactions on Geoscience and Remote Sensing, Vol. GE-23 No. 5 pp. 731-736.

Richardson, A.J., and C.L. Wiegand. 1977. "Distinguishing vegetation from soil background information," Photogrammetric Engineering and Remote Sensing, Vol. 43, pp. 1541-1552.

Sadowski, R., and M.J. Abrams. 1983. " Mapping of Hydrothermal Alteration Using Aircraft VNIR Scanners at the Posemont Porphyry Copper Deposit," Proceedings of the International Symposium on Remote Sensing of Environment, Second Thematic Conference, Remote Sensing for Exploration Geology, December 6-10, Ft. Worth, TX, pp. 175-188.

Salomonson, V.V., P.L. Smith, A.B. Dark, W.C. Webb, and T.J. Lynch. 1980. " ," IEEE Transactions on Geoscience and Remote Sensing, Vol. GE-18, no. 2, pp. 137-146.

Salomonson, V.V., Jackson, T.J., Lucus, J.R., Moore, G.K., Rango, A., Schmugge, T., and Scholty, D. (1983). "Water Resources Assessment," Colwel, R.N., (Ed.) Ch. 29, Manual of Remote Sensing. American Society of Photogrammetry.

Shibayama M. and C.L. Wiegand. 1985. "View Azimuth and Zenith, and Solar Angle Effects on Wheat Canopy Reflectance," Remote Sensory of Environment, Vol. 18, pp. 91-103.

Shih, E.H.H. and R.A. Schowengerdt. 1983. "Classification of Arid Geomorphic Surfaces Using Landsat Spectral and Textural Features," Photogrammetric Engineering and Remote Sensing, Vol. 49, pp. 337-347.

Smith, J.A. 1983. "Matter-Energy Interaction in the Optical Region," Colwel, R.N., (Ed.) Ch. 3, Manual of Remote Sensing. American Society of Photogrammetry.

Smith, J.A. 1983. "Refectance Models and Field-Measurements - Some Issues," Proceedings of the Society of Photo-Opical Instrumentation Engineers, Vol. 356, pp. 131-137.

Tucker, C.J., R.G. Townshend, and T.E. Goff. 1985. "African Landcover Classification Using Satellite Data," Science, Vol. 227, pp. 369-375.

Ustin, S.L., B.N. Rock and R.A. Woodward. 1985. "Analysis of Substrate and Plant Spectral Features of Semi-Arid Shrub Communities in the Owens Valley, California," Proceedings of the International Symposium on Remote Sensing of Environment, Fourth Themetic Conference, Remote Sensing for Exploration Geology, San Francisco, California, April 1-4. 13 pp.

Verhoef W. 1985. "Earth Observation Modeling Based on Layer Scattering Matrices," Remote Sensing of Environment, Vol. 17, pp. 160-178.

Walker, R.E., A.L. Zobrist, N.A. Bryant, B. Gokhman, S.Z. Friedman, and T.L. Logan. 1984. "An Analysis of LANDSAT-4 Themetic Mapper Geometric Properties," IEEE Transactions on Geoscience and Remote Sensing, Vol. GE-22, No. 3, pp. 228-293.

Walthall, C.L., J.M. Norman, Wells, G. Campbell, and B.L. Blad. 1985. "Simple Equation to Approximate the Bidirectional Reflectance From Vegetation Canopies and Bare Soil Surfaces," Applied Optics, Vol. 24, pp. 383-387.

Wardly, N.W. 1984. "Vegetation Index Variability as a Function of Viewing Geometry," International Journal of Remote Sensing, Vol. 5, no 5, pp. 861-870.

Weszka, J., C. Dyer, and A. Rosenfeld. 1976. "A Comparative Study of Texture Measures for Terrain Classification," IEEE Transactions on System, Man and Cybernetics, SMC-6, pp. 269-285.